NTNU – Trondheim
Norwegian University of
Science and Technology

Ultrasound Radiation Force for Increased Transport of Drugs in Cancer Tumors

Siri Vea

Master of Science in Cybernetics
Submission date: June 2014
Supervisor: Bjørn Atle J. Angelsen, ITK

Norwegian University of Science and Technology
Department of Engineering Cybernetics

Problem Description

When ultrasound is absorbed and scattered in an object, a radiation force is generated on the object. This force has a similar effect on material transport as a pressure gradient.

The task is to theoretically and experimentally explore the effect of such a radiation force in order to enhance the transport of chemotherapeutic drugs from the capillaries and through the extracellular matrix (ECM) (Interstitium) in cancer tumors. The drug can appear in free molecular form or encapsulated in nanoparticles. Experimental studies are conducted in a prostate cancer model in mice. The candidate should explore options for ultrasound equipment which can be used for *in vivo* experiments. The generated ultrasound radiation force should also be explored theoretically by use of existing simulation tools. Simulations should be used in order to decide an efficient scanning strategy which generates large forces without heat generation in the tissue.

Experiments in mice are conducted in cooperation with Professor Catharina de-Lange Davies' group at the Department of Physics.

Abstract

Cancer is today one of the leading causes of death world wide. Chemotherapy is a cancer treatment where cytotoxic drugs are administered intravenously in order to kill the cancer cells. This is a therapy form which is widely used, although it has large side effects and thereby greatly reduces the quality of life for the patients. Some of the main challenges with chemotherapy is that a large fraction of the dose is distributed in healthy tissue, and that the drug does not reach all cells in the tumor. Ultrasound waves generate a radiation force on the medium they propagate through. This force acts similar to a pressure gradient and can enhance transport of macromolecules from the capillaries and through the extracellular matrix (ECM) in tumors. By encapsulating the drug in larger particles, one can limit the concentration of drugs in healthy tissue, while ultrasound radiation force can enhance the concentration in the tumor. An *in vivo* experiment to investigate this effect was planned and conducted. Simulations of ultrasound waves that propagate through water and tissue show that appropriate ultrasound transducers can generate large radiation forces and potentially increase transport from capillaries to central regions of solid tumors significantly. However, the results from the conducted *in vivo* experiment must be analysed before any conclusions can be drawn. These results were not available during writing.

Sammendrag

Kreft er i dag en av de vanligste dødsårsakene i verden. Kjemoterapi er en form for kreftbehandling hvor cytotoksiske medikamenter gis intravenøst for å drepe kreftceller. Dette er en terapiform som er mye brukt, til tross for at den har store bivirkninger og dermed i stor grad reduserer livskvaliteten til pasientene. Noen av hovedutfordringene med kjemoterapi er at store deler av medikamentdosen havner i friskt vev, og at medikamentet ikke når frem til alle cellene i svulsten. Ultralydbølger genererer en strålingskraft på det mediet de forplantes gjennom. Denne kraften virker tilsvarende som en trykkgradient og kan øke transporten av makromolekyler fra kapillærer og gjennom den ekstracellulære matrise (ECM) i svulster. Ved å innkapsle medikamentene i større partikler, kan man begrense konsentrasjonen av medikamentene i friskt vev, mens ultralyd strålingskraft kan øke konsentrasjonen i svulsten. Et *in vivo* eksperiment for å undersøke denne effekten ble planlagt og gjennomført. Simuleringer av ultralydbølger som forplanter seg gjennom vann og vev viser at egnede ultralydtransducere kan generere store strålingskrefter og potensielt øke transporten fra kapillærene til sentrale områder av faste svulster. Men, før noen konklusjoner kan trekkes, må resultatene fra det gjennomførte *in vivo* eksperimentet analyseres. Disse resultatene var ikke tilgjengelige da dette ble skrevet.

Acknowledgements

I would like to express my special appreciation to my supervisor, Professor Bjørn Angelsen, for his passion and interest in my work, and for including me in a serious research project. He has always been available and gladly shared his knowledge with me. His spirit and positivity is truly inspiring. I would also like to express my gratitude to Ph.D candidate Ola Finneng Myhre, who has been helping me a lot throughout the semester. I would like to thank him for all the good discussions we have had, all the time he has spent on my project, and for the invaluable input he has given me in the process of writing this thesis.

I would also like to thank Professor Catharina deLange Davies and her research group at the Department of Physics, for letting me take part in the planning and completion of the *in vivo* experiment. A special thanks to Postdoc. Mercy Afadzi who was in charge of this.

Contents

List of Figures

List of Tables

Nomenclature

ECM	Extracellular Matrix
EPR	Enhanced Permeability and Retention
HIFU	High Intensity Focused Ultrasound
IFP	Interstitial Fluid Pressure
NP	Nanoparticle
PRF	Pulse Repetition Frequency
UMDD	Ultrasound Mediated Drug Delivery
URF	Ultrasound Radiation Force
VEGF	Vascular Endothelial Growth Factor

Chapter 1

Introduction

Cancer is today the leading cause of death in economically developed countries and the second leading cause of death in developing countries[1]. Although cancer treatment has improved in recent years, the mortality rates remain high, especially for certain cancer sites, like the pancreas. Cancer-causing behaviours like smoking and a fatty diet, in combination with an ageing population, cause the cancer incident rates to continuously increase.

1.1 Motivation

Cancer is commonly treated with surgery, radiation therapy and chemotherapy, although the range of treatment types has expanded greatly during the past decades. A combination of two or more of these treatment types is often used. Surgery is for example often followed by chemotherapy in order to ensure that no cancer cells remain in the body. Chemotherapy treatment has two purposes; it shall prevent cancer cell proliferation, have a *cytostatic* effect, and kill the cancer cells, have a *cytotoxic* effect. The aim is to achieve this with minimal side effects. The effectiveness of a drug is indicated by its therapeutic index, which is the ratio between the maximum tolerated dose which can be delivered to the body, and the minimum effective dose which is needed in order to gain a therapeutic effect. Chemotherapeutic drugs have very low therapeutic indices; the minimal effective dose can in some cases be lethal.

Chemotherapeutic drugs are administrated intravenously in molecular form. The small molecular sizes enable the drugs to leave the blood flow through the capillaries in both healthy and cancerous tissue. This implies that in order to ensure that a minimal effective dose is delivered at the tumor site, the rest of the body is exposed to a corresponding dose. The side effects of the chemotherapy treatment greatly reduce the quality of life for cancer patients. Researchers therefore aim to allow chemotherapeutic drugs to be delivered and absorbed locally, in order to minimize the side effects of the therapy and increase the patients' quality of life.

This thesis presents opportunities for cancer treatment using a combination of ultrasound and chemotherapeutic drugs, and presents an overview of a conducted *in vivo* experiment where this was tested in mice. The idea is to encapsulate the chemotherapeutic agent in drug carriers with diameter of approximately 3 to 100 nm. Such nanoparticles (NPs) are too large to penetrate the capillary walls in healthy tissue, and will therefore reduce the side effects of the therapy, as only a limited amount of the drug will reach other areas than the tumor. Capillary walls in tumor tissue have larger intracellular spaces than capillaries in healthy tissue, which enable the large drug carriers to extravasate into the tumor interstitium. In this way, the chemotherapeutic treatment will be local, and the therapeutic index will increase. There are, however, many challenges associated with this approach. Transport of macromolecules across the capillaries in tumor tissue is slow due to elevated pressure in the tumor interstitium. Many tumors have necrotic and hypoxic areas, and the vascular density is strongly heterogeneous. In order to enhance the transport across the vessel walls and to deliver the drug also to areas with low vascular density, the idea is to apply ultrasound.

Ultrasound waves are sound waves with frequencies above the hearing range, i.e. larger than 20 kHz. The waves are longitudinal, mechanical waves which require a medium in order to propagate. As ultrasound waves propagate through tissue, the tissue is alternately compressed and expanded. In this process, some of the energy of the wave is lost to scattering and absorption. Change in the momentum of the wave generates a net force in the propagation direction. This force is called the ultrasound or acoustic radiation force, and has in recent years been studied as a mean to enhance transport of drugs across the capillary walls in solid tumors [2].

1.2 Structure of the thesis

Encapsulating chemotherapy in nanoparticles in combination with application of ultrasound is an approach towards targeted drug delivery, in order to increase the therapeutic index of chemotherapy. *In vitro* experiments have shown that ultrasound radiation force is able to create streaming of particles towards the vessel walls in areas of high flow [3]. Also *in vivo* experiments show promising results in local delivery of cytotoxic drugs to tumors [2]. However, thorough *in vivo* verification is needed before this concept can be introduced to the clinic. This thesis aims to introduce the reader to the concept of ultrasound mediated drug delivery and how this can be verified in an *in vivo* experiment in mice. The thesis is structured in the following manner:

- **Chapter 2** presents a theoretical background of tumor biology and ultrasound physics.
- **Chapter 3** presents key factors and parameters to consider when designing an experiment to investigate the effects of ultrasound on delivery of nanoparticles to tumors in mice.
- **Chapter 4** presents simulations of ultrasound wave propagation and generated radiation force, in order to choose the appropriate ultrasound equipment and decide on a physical set-up.
- **Chapter 5** presents the conducted *in vivo* experiment.

- **Chapter 6** discusses an experimental set-up with respect to the simulated wave fields and the conducted *in vivo* experiment.

- **Chapter 7** presents conclusive remarks and outlines further work in the field of ultrasound mediated drug delivery.

Due to considerable delays in the delivery of transducers for the *in vivo* experiment, the results from the experiment are not yet analysed and will not be presented in this thesis. The focus is therefore rather on how one can design a similar experiment of high quality for further investigation of these phenomena in the future.

Chapter 2

Background: Cancer biology and ultrasound physics

In order to understand the concept of ultrasound mediated drug delivery (UMDD), the reader will be introduced to some of the biological properties of cancerous tissue and physical properties of ultrasound wave propagation.

2.1 Tumor growth

Tumors are results of cell mutations which induce rapid cell division. A cancerous tumor starts with one mutated cell which proliferates abnormally. The resulting two cells in turn proliferate into four cancerous cells, leading to an exponential growth rate. This rapid cell division and growth requires increased supply of oxygen and nutrition, which serves the need for vascular recruitment.

Two genes are especially important in tumor development and growth: the proto-oncogenes, and the tumor suppressor genes [4]. Proto-oncogenes are genes which encode proteins that are involved in the regulation of cell growth and proliferation, while tumor suppressor genes encode proteins that in some way inhibit cell proliferation. Mutations in these genes are common initiators to cancer.

Mutations in the proto-oncogenes lead to overstimulation of the growth promoting machinery in the cell. Growth factor receptors attached to the surface of the cell normally fire a growth signal to the cell nuclei when stimulated by a growth factor released from a neighbouring cell. In a similar manner, inhibitory brigades attached to the cell surface react to growth blocking signals and fire an inhibitory signal when stimulated. Mutations in the gene expressions enable the growth factor receptors to fire even though they are not stimulated from the outside, and inhibitory brigades to ignore growth blocking signals from neighbouring cells [5]. In many types of cancer cells, critical components of these brigades are inactive or absent.

It is the cell cycle clock that receives the growth promoting and inhibitory signals. Based on the received signal, the cell cycle clock decides whether the cell should move on in its life cycle or not. The clock is often deranged in cancer cells. This, in combination with bombardments of growth factors and limited signals from growth inhibitors, leads to rapid cell growth and division.

2.1.1 Tumor vasculature

As the tumor grows, the need for oxygen and nutrition increases. This causes tumor angiogenesis, the process of growth and formation of new blood vessels based on signals and actions induced by the tumor and the tumor microenvironment [6]. Tumor angiogenesis is one of the six hallmarks of cancer; it is an indication of malignant development of a tumor [7]. In order to recruit and grow new vasculature, vascular endothelial growth factors (VEGFs) are essential, and overexpressed in most tumor types [6]. VEGFs are glycoproteins which induce both vascular permeability and endothelial cell proliferation [8, 9]. Endothelial cells are cells which form the endothelium, the interior surface of blood vessels. These cells have VEGF receptors which react when stimulated by VEGFs, leading to a series of events which result in blood vessel formation [6]. In addition, VEGFs can increase the vascular permeability, allowing leakage of plasma proteins from the blood vessels and formation of an extra-vascular matrix. This further enhances the environment for endothelial cell growth, as the extra-vascular matrix scaffolds the cells and formation of new vessels. An over-expression of VEGFs will therefore lead to rapid formation of new vasculature. VEGFs are among others released from tumor cells which are oxygen-deprived.

Blood supply in healthy tissue is ensured by a structured and efficient vascular network, with an hierarchic architecture. The main arteries are parallel to the main veins, with intermediate arterioles, capillaries and venules. In contrast to this, tumor vasculature is chaotic. Since tumor angiogenesis is a result of uncontrolled release of VEGFs, the resulting vasculature is highly tortuous. There is no conventional hierarchy structure, and this lack of structure makes distinction of capillaries, arterioles and venules hard. The resulting blood flow is difficult to predict. Loops and tortuous formations also increase the vessels' resistance to blood flow.

In addition to total lack of vascular structure, tumor vasculature is characterized by altered structure of the vessel walls. Due to the increased release of VEGFs, the endothelial cell proliferation is also increased. Healthy vascular structures include perivascular cells and protein complexes that cover the endothelial cell layer and stabilize the vessel. This coverage lacks in tumor vasculature, resulting in large intercellular spaces and leaky vessel walls [6]. There are larger gaps between the endothelial cells, which allow for transport of macromolecules through the fenestrae of the vessel wall. The altered structure also leads to leakage of blood plasma into the interstitium, which results in an elevated interstitial fluid pressure (IFP). Tumors often have limited lymphatic drainage, which also contributes to increased IFP. Increased IFP can cause occlusion of the vessels and thereby lead to hypoxia, which results in persistent release of VEGFs.

In healthy tissue, transport of macromolecules across the capillary walls is normally governed by convection and diffusion. Diffusion is mass transport driven by the concentration gradient, while convection is mass transport driven by the pressure gradient. The capillary blood pressure is larger than the pressure in the surrounding tissue, which creates a pressure gradient from the vessels and into the interstitium. The increased IFP in tumors eliminates this gradient partly or fully. This makes transport across the vessel walls slow in tumor tissue, as diffusion is the only transport initiating mechanism. Tumor blood flow is not laminar, but rather turbulent. Molecules may therefore also circulate within the center of the blood stream, without reaching the vessel wall and be able to extravasate into the surrounding tissue.

2.1.2 The Enhanced Permeability and Retention Effect

In tumor tissue, leaky vasculature enables macromolecules to travel across the capillary walls, while altered lymphatic drainage enables them to remain and accumulate there [10]. This is recognized as the enhanced permeability and retention (EPR) effect . Possibilities for selective intervention and drug targeting based on the EPR effect have been studied as a new approach towards local tumor treatment [11, 12]. Nanosized macromolecules are, due to their size, able to escape renal clearance. They are also too large to penetrate the capillary walls of healthy tissue. Due to intercellular fenestrae in tumor vasculature, macromolecules can leave the blood stream at the tumor site and get trapped in the tumor interstitium. Altered lymphatic drainage leads to aggregation of these molecules over time. This process is, however, slow, because the high IFP decreases the pressure gradient in tumors, as described in the previous section.

2.1.3 Extracellular Matrix

The tumor cells are connected by the extracellular matrix (ECM), which is a complex network of biochemical components. These include proteins, glycoproteins, proteglycans and polysaccharides [13]. In healthy tissues, the ECM is structured, and the network of components with different physical, biochemical and biomechanical properties is essential in regulating cell behaviour. The rigidity, porosity, spatial alignment and orientation of the ECM components, all contribute to the physical properties of scaffolding the surrounding tissue. At cancer sites, the structure of the ECM becomes disorganized, and it can be a contributor to cell proliferation and metastasis [14].

In an UMDD perspective, the permeability of the ECM in tumors is of interest, as it is desirable that drug loaded particles are able to penetrate the ECM by application of an ultrasound pressure wave. It is shown that the stiffness of the ECM is correlated with the total tissue content of collagen, and that tumor tissue is more rigid than healthy tissue [15]. Large collagen content contributes to a lower compliance, which makes the tissue more penetration-resistant to macromolecules than normal tissue [16]. Collagen fibres can also physically hinder the transport of a particle through the ECM, if the particle is larger than the spacing between the fibres.

It is also of interest whether cancerous ECM has thixotropic properties or not. Thixotropic fluids are fluids which are thick under static conditions, and become less viscous when stirred. If this is the case for tumor ECM, an external force above a certain threshold is required to be able to move particles within the ECM. However, when particle movement is initiated, the ECM will be less viscous, which enables a smaller force to keep the particle moving. If the ECM does not possess this property, a smaller external force applied over a longer time will have the same effect, and it will then be the total force impulse which determines the length of the particle movement. Basement membranes are extra-cellular matrices surrounding endothelial and epithelial cells, for example extra-vascular matrices. In general, basement membranes hold thixotropic properties [17], but since the ECM structure and composition is altered in tumors, it is not known whether this property is valid for tumor basement membranes and tumor ECM.

2.2 Ultrasound Physics

Ultrasound waves are sound waves with frequencies above the hearing range, i.e. above 20 kHz. The waves are longitudinal, mechanical waves which require a medium in order to propagate. For medical applications, ultrasound with frequencies in the range of $1 - 50\,\mathrm{MHz}$ is normally used. Ultrasound in medicine is used as a diagnostic imaging method or for treatment purposes.

As ultrasonic waves propagate in tissue, the tissue is alternately compressed and expanded as the energy alternates between kinetic and potential energy states. Inhomogeneities in the tissue lead to energy absorption and scattering of the wave. These two factors reduce the amplitude of the wave as it propagates deeper into tissue.

2.2.1 Linear propagation

In order to model wave propagation in a medium, equations which describe the interactions between the pressure wave and the medium it propagates through are needed. We assume that the pressure wave acts on a volume V. The vibrations in the wave motion can be described by the displacement, $\vec{\Psi}(\vec{r}, t)$, of a particle from its equilibrium position $\vec{r}$. If we choose a volume $V = \Delta V$ so small that $\nabla\vec{\Psi}$ is approximately constant over the volume, we can approximate the volume change by

$$\partial V = \nabla\vec{\Psi}(\vec{r}, t)\Delta V \tag{2.1}$$

This is illustrated in figure 2.1. Hence, the relative volume change is

$$\frac{\partial V}{\Delta V} = \nabla\vec{\Psi} \tag{2.2}$$

If now a linear, non-viscous relationship between the pressure and volume compression is assumed, this can be described by

$$p = -\frac{1}{\kappa}\frac{\partial V}{\Delta V} = -\frac{1}{\kappa}\nabla\vec{\Psi} \qquad\qquad \frac{\partial p}{\partial t} = -\frac{1}{\kappa}\nabla\vec{u} \tag{2.3}$$

where $\vec{u}$ is the particle velocity and κ is the compressibility of the medium[18]. The conservation equation for momentum in Lagrange variables can be written

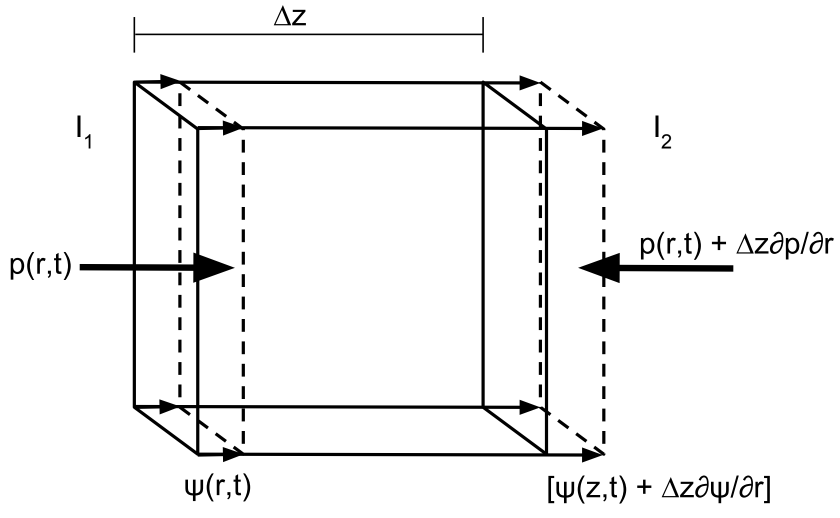

FIGURE 2.1: Volume change of a small element caused by wave motion

$$\rho\frac{\partial\vec{u}(\vec{r},t)}{\partial t} = -\nabla p(\vec{r},t) \tag{2.4}$$

where it is assumed that no other forces are acting on the tissue than those caused by the compression of the tissue from the wave itself. However, the wave needs to be generated by external forces acting on the tissue. We therefore add an extra force $\vec{f}$ per unit volume to the momentum equation

$$\rho\frac{\partial\vec{u}(\vec{r},t)}{\partial t} = -\nabla p(\vec{r},t) + \vec{f}(\vec{r},t) \tag{2.5}$$

Applying the ∇-operator to this equation yields

$$\rho\frac{\partial\nabla\vec{u}(\vec{r},t)}{\partial t} = -\nabla^2 p(\vec{r},t) + \nabla\vec{f}(\vec{r},t) \tag{2.6}$$

Substitution of $\vec{u}(\vec{r},t)$ from equation (2.3) gives us the wave equation i three dimensions

$$\nabla^2 p(\vec{r},t) - \rho\kappa\frac{\partial^2 p(\vec{r},t)}{\partial t^2} = \nabla\vec{f}(\vec{r},t) \tag{2.7}$$

If linear propagation is assumed, ultrasonic wave propagation can be described by the inhomogeneous wave equation in its general form:

$$\nabla^2 p(\vec{r},t) - \frac{1}{c^2}\frac{\partial^2 p(\vec{r},t)}{\partial t^2} = -s(\vec{r},t) \qquad c = \sqrt{\frac{1}{\rho\kappa}} \tag{2.8}$$

where $p(\vec{r},t)$ is the pressure amplitude, $c = \sqrt{\frac{1}{\rho\kappa}}$ is the speed of sound in tissue, and $-s(\vec{r},t)$ is a source term that can represent linear scattering.

Figure 2.2 shows an ultrasound pulse at focus generated by a linear simulation of a 10 MHz ultrasound pulse. The parameters used in the simulation are given in table 2.1.

Table 2.1: Simulation parameters for linear simulation

Simulation parameters	
Center frequency	10 MHz
Aperture	Circular
Aperture width	19 mm
Pulse length	0.5 µs
Focus	50 mm
Water propagation	40 mm
Initial pressure	200 kPa

The propagation equation does not involve any quadratic or higher order terms, which implies that the frequency components will not change as the wave propagates. This can clearly be seen from the frequency spectrum in figure 2.2, as all the energy is situated around the center frequency, and the pulse form is not distorted.

2.2.2 Non-linear propagation

Human tissue does also have non-linear properties, that is, the compressibility, κ, and the density, ρ, change with applied pressure. In order to govern a non-linear

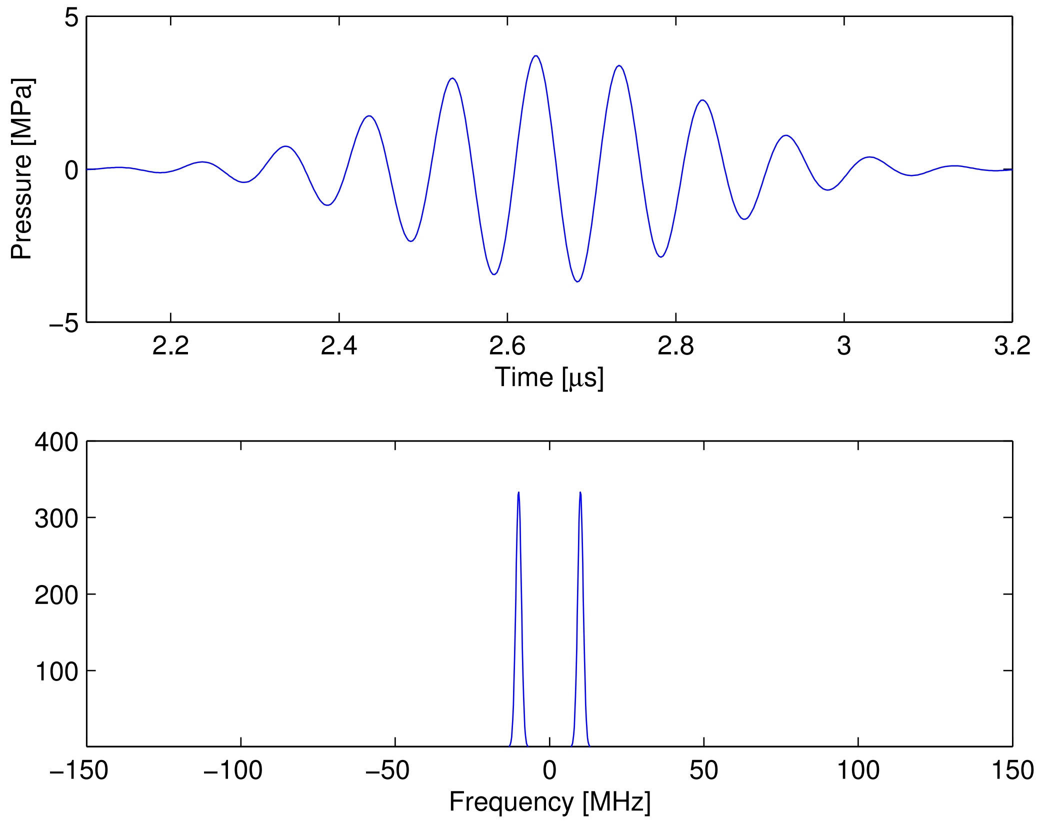

FIGURE 2.2: A 10 MHz pulse at focus in 50 mm simulated with linear propagation through water and soft tissue.

wave equation, we introduce the tissue density, $\rho(\vec{r})$, and compressibility, $\kappa(\vec{r})$, at the equilibrium position, $\vec{r}$. A material relation which accounts for non-linear elasticity and linear loss is given by [19]:

$$-\nabla \cdot \vec{\Psi}(\vec{r},t) = \kappa(\vec{r})\rho(\vec{r}) - \beta_n(\kappa(\vec{r})p(\vec{r},t))^2 - \kappa(\vec{r})\mathcal{L}p(\vec{r},t) \tag{2.9}$$

where β_n is the coefficient of non-linearity and $\mathcal{L}$ is a convolution kernel accounting for frequency dependent absorption. Combining this with the relation

$$\vec{u} = \frac{\partial \vec{\Psi}}{\partial t} \tag{2.10}$$

and equation (2.4) yields a generalized Westerwelt equation for non-linear propagation in tissue [19, 20]:

$$\kappa\frac{\partial^2 p}{\partial t^2} - \nabla\cdot(\frac{1}{\rho}\nabla p) = \frac{\partial^2}{\partial t^2}(\beta_n\kappa^2 p^2 + \kappa L p) \tag{2.11}$$

The non-linearity-term

$$\frac{\partial^2}{\partial t^2}\beta_n\kappa^2 p^2 \tag{2.12}$$

introduces a pressure dependent pulse form distortion. When the tissue is compressed, the compressibility decreases, in turn causing the speed of sound to increase due to the relation $c = \frac{1}{\sqrt{\rho\kappa}}$. This results in faster propagation of the wave peaks than the wave troughs, causing a saw-tooth waveform as the wave propagates. This non-linear waveform distortion transfers energy from the fundamental band to higher harmonic components.

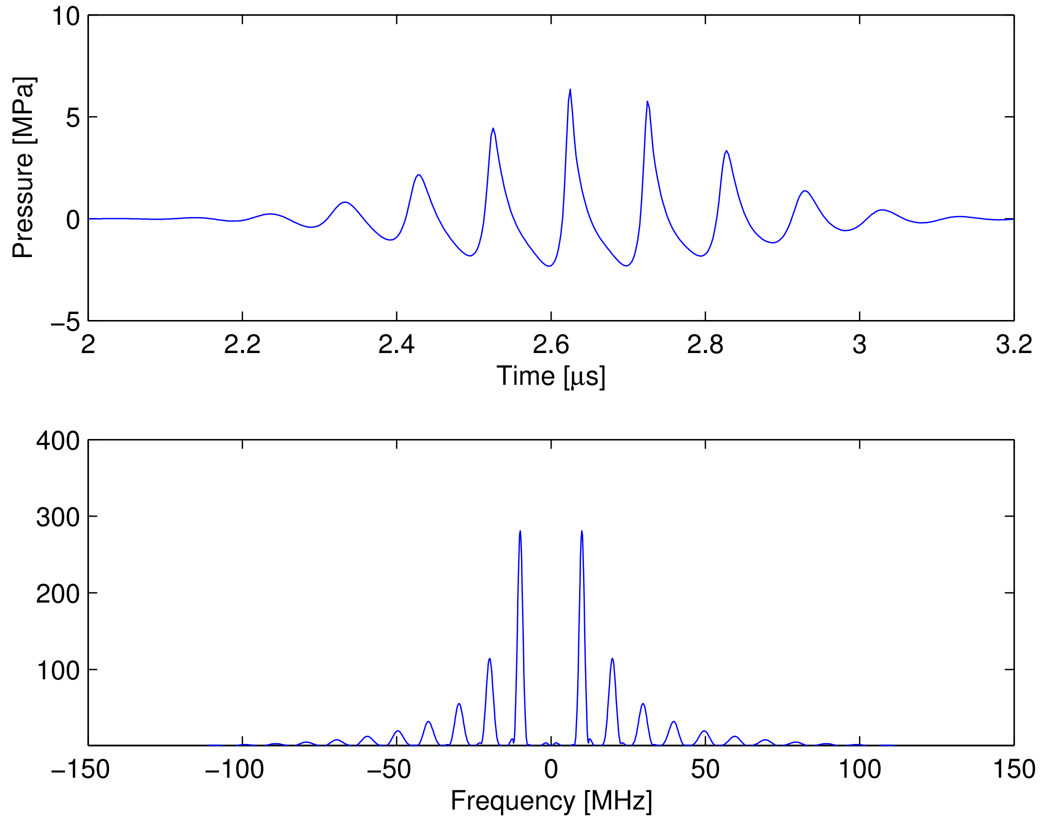

FIGURE 2.3: A 10 MHz pulse at focus in 50 mm simulated with non-linear propagation through water and soft tissue.

Figure 2.3 shows a 10 MHz ultrasound pulse at focus generated by a non-linear simulation [21]. The parameters in this simulation are the same as the parameters in the linear simulation (see table 2.1) shown in figure 2.2. From the non-linear simulation we can clearly see the distortion of the pulse, both from the time and frequency domain plots. The pulse form has sharp peaks, and the energy is pumped into harmonic and sub-harmonic components. The distorted waveform appears in focus due to higher harmonic components which are out of phase.

An important aspect is that both the non-linear and linear simulations shown are generated by simulating propagation through water before the wave reaches tissue. Water is a material with almost no attenuation, that is, the higher frequency components are not absorbed, and energy will continue to be pumped into higher harmonics. Soft tissue in the body is however attenuating, and both the amplitude and the frequency components will to a large extent be reduced. This is illustrated

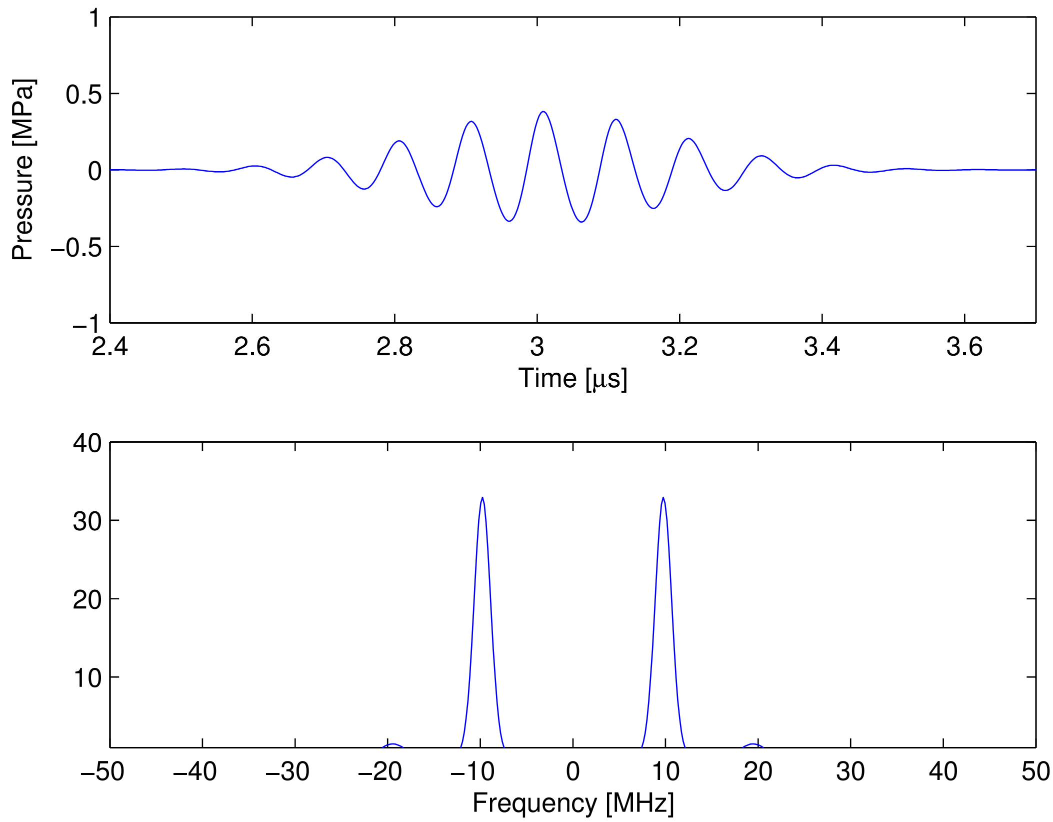

FIGURE 2.4: A 10 MHz pulse at focus in 50 mm simulated with non-linear propagation through 50 mm soft tissue. The rest of the simulation parameters are similar to the parameters listed in table 2.1.

in figure 2.4. From this simulation one can clearly see that almost all the energy in the wave is attenuated. Even though the beam is focused, the pressure in focus is very low and only the second harmonic is barely present in the frequency spectrum. The higher harmonic components are attenuated, and the resulting waveform is very close to a sinusoid.

2.2.3 Focusing and diffraction of beams

Ultrasound beams can either be focused or unfocused, depending on the curvature of the transducer surface. If the transducer surface is flat, the beam will be unfocused. If the transducer surface is curved with a radius r, the focal point will lay in the point which has the distance r to all points on the transducer surface. The area around the focal point is called the focal zone. In this area, the pressure amplitudes will add constructively and create the largest pressures and intensities in the sound field. The size of the focal zone is dependent both on the F-number, $F_{\#}$, and the frequency. The F-number is the relation between the focus depth, z_f, and the aperture size, D, of the transducer

$$F_{\#} = \frac{z_f}{D} \tag{2.13}$$

and is used as a relative measurement of how focused the transducer is. The lower F-number, the more focused is the beam and vice versa. The $-3\,\mathrm{dB}$ length and width of the focal zone is approximated by [18]

$$D_f \approx F_{\#}\lambda = \frac{z}{D}\lambda \qquad \text{and} \qquad L_f \approx 4\lambda F_{\#}^2 \tag{2.14}$$

The beam form of a focused beam is illustrated in figure 2.5. The wavefront is approximately planar in the focal zone. Focusing can also be achieved by a focusing lens, which can be attached to a flat transducer surface. Such an acoustic lens bends the sound waves in a similar manner as an optical lens bends light beams.

When an ultrasound wave is emitted from the transducer surface, it will be diffracted in the same way as light passing through a small opening. This is

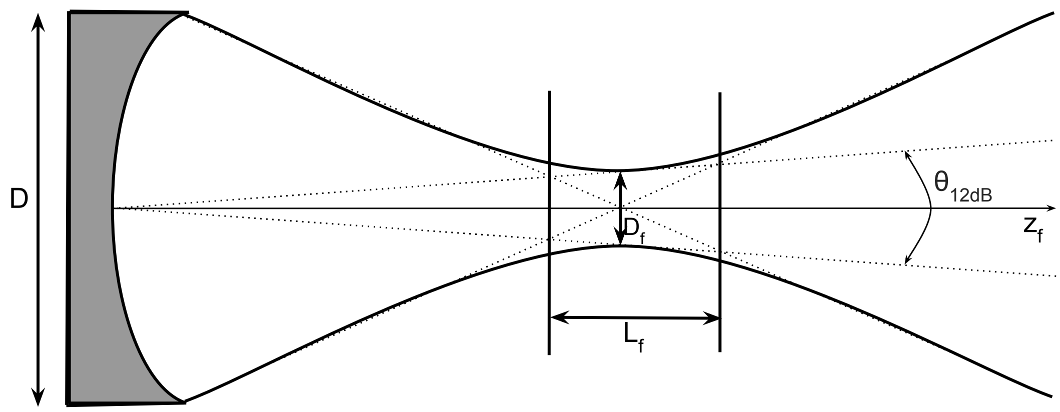

Figure 2.5: Illustration of transducer focusing.

due to the fact that the wave does not origin from a single point, but rather from many points along the surface of the piezoelectric element. The resulting sound field therefore consists of waves which interact and interfere with each other. At every point where the waves interact, the resulting amplitude of the particle displacement is the sum of the amplitudes of the interacting waves. If the waves are in phase, the result will be a larger amplitude. However, if the waves are out of phase, they will destructively interfere and cancel each other out. This diffraction pattern thus produces areas with larger amplitudes, but also areas of destructive interference and zero-points in the nearfield. In the focal zone, the waves sum up to one constructive interference field, which generates the largest pressure amplitudes in the field. For therapeutic purposes, it is important that the region of interest is not placed in any of the destructive interference zones.

2.2.4 Ultrasound Radiation Force

When an ultrasound wave propagates through tissue, it produces a net force on the volume it acts on. This force is called the ultrasound radiation force (URF) and is a result of transfer of momentum from the sound wave in an attenuating medium where the pressure and particle velocity become out of phase [22]. In order to mathematically model this force, continuum mechanics is useful.

Stress expresses the internal forces that neighbouring particles exert on each other in a continuous material. When a liquid is under pressure, each particle is pushed inwards by the surrounding particles, and, in reaction, pushes the surrounding particles outwards. At ultrasonic frequencies, soft tissues can be modelled as viscous fluids [23] and stress then represents the force per unit area that counteracts the applied external force. In terms of Cauchy's stress tensor, $\vec{\sigma}$, Newton's second law can be expressed by the Euler description as

$$f_i = \frac{\partial \sigma_{ij}}{\partial x_j} = \rho a_i \tag{2.15}$$

or in its invariant form

$$\vec{F} = \nabla \vec{\sigma} = \rho \vec{a} \tag{2.16}$$

where $\vec{F}$ is the externally applied force per unit volume and $\vec{a}$ is particle acceleration [24, pp. 134-136]

For a linearly viscous (Newtonian) fluid, the constitutive equation can be described by

$$\sigma_{ij} = -p\delta_{ij} + \left(k - \frac{2}{3}\mu_f\right) D_{kk}\delta_{ij} + 2\mu_f D_{ij} \tag{2.17}$$

where $D_{ij} = \frac{1}{2}\left(\frac{\partial u_i}{\partial x_j} + \frac{\partial u_j}{\partial x_i}\right)$ represents the rate of deformation, $\vec{u}$ the particle velocity and p is a scalar pressure. k and μ_f are material constants, representing bulk and shear viscosity, respectively.

Acceleration of a fluid particle is the sum of the local particle acceleration and the convection [25, pp. 128-130]:

$$\vec{a} = \frac{\partial \vec{u}}{\partial t} + (\vec{u} \cdot \nabla)\,\vec{u} \tag{2.18}$$

By combination of equations (2.15) and (2.18), the Navier-Stokes equation of motion is obtained. For a linearly viscous fluid, described by equation (2.17), Navier-Stokes equation reduces to

$$-\nabla p + \left(k + \frac{\mu_f}{3}\right)\nabla\left(\nabla \cdot \vec{u}\right) + \mu_f \nabla^2 \vec{u} = \rho\left(\frac{\partial u}{\partial t} + \left(\vec{u} \cdot \nabla\right)\vec{u}\right) \tag{2.19}$$

The solution to this equation can be approximated by a perturbation analysis [26, *Perturbation methods*, Jerry H. Ginsberg, pp. 279-308]. This involves expanding the density, pressure and velocity in terms of time-dependent approximations to the steady-state solutions, with higher-order time-independent correction terms. If terms up to second-order are kept, and the analysis is applied to the right-hand side of equation (2.19), the approximation leads to

$$\rho_0 \frac{\partial \vec{u}_2}{\partial t} + \frac{\partial \rho_1 \vec{u}_1}{\partial t} + \rho_0\left(\vec{u}_1 \nabla \cdot \vec{u}_1 + \vec{u}_1 \cdot \nabla \vec{u}_1\right) \tag{2.20}$$

where ρ_0 is the material density at equilibrium, $\vec{u}_1$ and ρ_1 are first order approximations for particle velocity and density, and $\vec{u}_2$ is a higher-order correction term representing the acoustic streaming velocity. This force represents the transfer of momentum from the wave to the attenuating material. If the temporal average of this expression is calculated, the first two terms will be zero, and the resulting equation reduces to:

$$\vec{F} = 2\rho\langle \vec{u}\vec{u}_{,z}\rangle \tag{2.21}$$

where the force is in the direction of the propagating wave, the z-direction. If exponential attenuation is assumed, the radiation force per unit volume can be expressed as

$$\vec{F} = \frac{\sigma_e(\omega)\vec{I}(\omega)}{c} \tag{2.22}$$

where σ_e is the acoustic intensity extinction cross section, $I(\omega)$ is the acoustic intensity and c the speed of sound in tissue. $\omega = 2\pi f$ is the angular frequency of the incident wave. The extinction cross section of the acoustic intensity is the sum of the scattering and absorbing cross sections

$$\sigma_e(\omega) = \sigma_s(\omega) + \sigma_a(\omega) = 2\alpha(\omega) \tag{2.23}$$

and is twice the pressure extinction cross section, $\alpha(\omega)$. Scattering is the re-direction of incident acoustic energy from the incident beam, while absorption is the conversion of acoustic energy into thermal energy. Note that the tissue in the above equations is considered a continuum, rather than discrete particles. This is an approximation, since tissue is strongly heterogeneous with gaps between neighbouring cells and interconnecting ECM. We have also assumed that the wavefront is planar. As described in section 2.2.3, this is a valid assumption in the focal zone.

Radiation force can also be described in a more intuitive way. This is illustrated in figure 2.6. If a wave is propagating in an attenuating medium, one can look at

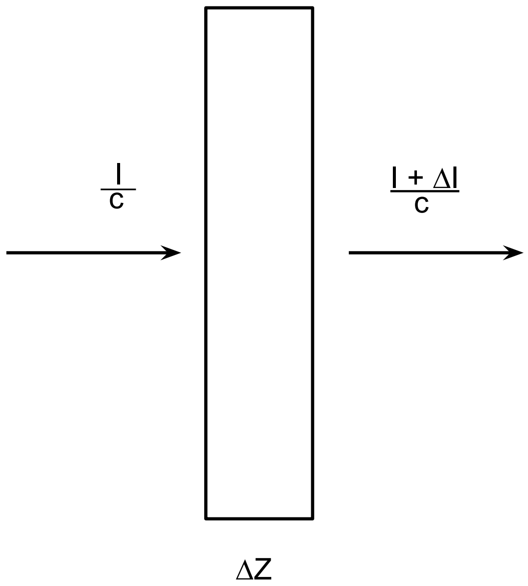

FIGURE 2.6: Illustration of generation of URF.

the propagation through a volume with size Δz in the propagating direction. The moment of the wave that enters the volume is then

$$\rho u_i^2 = \frac{\rho c}{c} u_i^2 = \frac{Z_0}{c} u_i^2 = \frac{I}{c} \tag{2.24}$$

where $Z_0 = \rho c$ is the characteristic acoustic impedance of the medium. The intensity is reduced by scattering and absorption within the volume element, and the moment of the wave which exits the volume is then

$$\rho u_o^2 = \frac{I + \Delta I}{c} \tag{2.25}$$

where the intensity lost in the volume is

$$\Delta I = -\sigma_e(\omega) I(\omega) \tag{2.26}$$

The change in moment per unit volume is force per unit volume, and hence the ultrasound radiation force can be expressed as

$$\Delta\vec{F} = \left(\frac{I(\omega)}{c} - \frac{I(\omega) + \Delta I(\omega)}{c}\right)\Delta V = \frac{\sigma_e(\omega) I(\omega)}{c}\Delta V \tag{2.27}$$

This is a similar expression to equation (2.22) derived by continuum mechanics.

A pressure $p(\vec{r}, t)$ acting on a surface S of a volume V produces a net force on the volume given by

$$\vec{F} = -\int_S d^2 r \vec{n} p(\vec{r}, t) = -\int_V d^3 r \nabla p(\vec{r}, t) \tag{2.28}$$

where $\vec{n}$ is the outward unit normal to the surface [27]. For a small volume ΔV, the integral can be approximated to

$$\Delta\vec{F} = -\nabla p(\vec{r}, t)\Delta V \tag{2.29}$$

When comparing this to equation (2.27), it can be seen that the radiation force has the similar form as a pressure gradient acting on a volume. As mentioned in section 2.1.2, the elevated interstitial fluid pressure in tumors decreases the pressure gradient which normally contributes to macromolecule transport across the capillary wall. UMDD is based upon the idea that URF can act similar to such a pressure gradient and thereby force drug loaded macromolecules across the tumor capillary walls and into the interstitium.

The intensity extinction cross section is dependent upon the frequency, and is generally larger for larger frequencies. Since a nonlinear simulation will generate higher harmonic and sub-harmonic frequencies, it is important to include this in the calculation and simulation of ultrasound radiation force. Another important aspect is that higher frequencies generate a narrower focal zone and thereby higher pressures and intensities, which in turn also contribute to higher radiation force output.

Pressures in the body are normally measured in mmHg. The radiation force is a force per unit volume, i.e. $\mathrm{N/m^3}$. These units relate in the following manner:

$$1\,\mathrm{mmHg} \sim \rho_{Hg} g h = 13.546 \cdot 10^3 \frac{\mathrm{N}}{\mathrm{m}^3} \cdot 9.81\,\frac{\mathrm{m}}{\mathrm{s}^2} \cdot 10^{-3}\mathrm{m} = 132.9\,\frac{\mathrm{N}}{\mathrm{m}^2} = 132.9\,\mathrm{Pa} \tag{2.30}$$

This means that a radiation force per unit volume corresponds to

$$1\frac{\mathrm{N}}{\mathrm{m}^3} = \frac{1}{132.9}\frac{\mathrm{mmHg}}{\mathrm{m}} = 7.524 \cdot 10^{-3}\frac{\mathrm{mmHg}}{\mathrm{mm}} \tag{2.31}$$

2.2.5 Ultrasound Tissue Heating

As described in the previous section, a part of the wave intensity is attenuated as the wave propagates through tissue. Along a line in the z-direction, the change can be described as

$$dI = -\sigma_e(\omega) I(\omega) dz \tag{2.32}$$

If we assume plane wave propagation, the relation between the pressure and intensity is

$$I = \frac{P^2}{2Z_0} \tag{2.33}$$

where Z_0 is the acoustic impedance of the medium. The change in intensity can therefore be described as

$$dI = \frac{d}{dP}\left(\frac{P^2}{2Z_0}\right) = \frac{PdP}{Z_0} = -\sigma_e \frac{P^2}{2Z_0} dz \tag{2.34}$$

Which gives the relation

$$dP = -\frac{\sigma_e(\omega)}{2} P dz \tag{2.35}$$

At a point z, the intensity and pressure can be expressed as

$$I(z,\omega) = I_0 e^{-\sigma_e(\omega) z} \qquad P(z,\omega) = P_0 e^{\frac{-\sigma_e(\omega)}{2} z} \tag{2.36}$$

As described in equation (2.23), $\sigma_e(\omega) = 2\alpha(\omega)$, where $\alpha(\omega)$ is the amplitude attenuation coefficient, which is the sum of the amplitude scattering and absorption coefficients, $\alpha = \alpha_a + \alpha_s$ [28]. In tissue a typical value is $\alpha = 0.5\,\mathrm{dB/cmMHz}$ [18]. Only the absorption contributes to heat generation. If the tissue has an absorption coefficient α_a, the generated heat per unit volume [W/m^3] can be found by differentiation of equation (2.36) as

$$\vec{q_v} = -\frac{dI(\vec{z})}{dz} = 2\alpha_a I(\vec{z}) \tag{2.37}$$

Penne's bio-heat equation models the heat distribution in tissue [29, 30] as

$$\rho C \frac{\partial T}{\partial t} = k\nabla^2 T - W_b C_b T + q \tag{2.38}$$

where ρ is tissue density, C is the specific heat of the tissue, k is the thermal conductivity and T is the temperature. The term $W_b C_b T$ accounts for blood perfusion, where W_b is the perfusion rate and C_b the specific heat of blood. q is the heat generated in tissue. Since the heat generated in the tissue by metabolic activity is much lower than that generated by the ultrasound absorption, it can be ignored, i.e. $q \approx q_v$.

Tissue heating is a safety issue in medical ultrasound applications. High intensity focused ultrasound (HIFU) treatment utilizes the generated heat from high intensity beams to ablate pathological tissue at temperatures around 60 °C. In ultrasound imaging applications, tissue heating is strictly regulated. Hyperthermia is considered to be any temperature above 40 °C, and temperatures above 45 °C alters the tertiary structure of proteins and is lethal to most organs and organisms

[31]. The American Food and Drug Administration (FDA), limits the acoustic output from commercial imaging transducers to 720 mW/cm^2, which corresponds to a temperature rise of maximum 2 °C in tissue [32].

2.3 Ultrasound Transducer Properties

Commercial ultrasound transducers are normally built up by a stack of piezoelectric ceramic layers with backing and matching layers in back and front of the piezoelectric elements. The characteristics of the chosen ultrasound transducer are of high importance when considering an ultrasound mediated drug delivery scheme. In order to get the desired output, the transducer needs to be optimized for the desired purpose.

2.3.1 Bandwidth and efficiency

Transducer bandwidth is the range of the frequency band where the transducer operates within −3 dB of the output at the fundamental frequency. Imaging transducers normally have larger bandwidths than therapy transducers. This is due to the fact that bandwidth and efficiency is closely connected. In order to obtain larger bandwidths, the piezoelectric elements are sliced in smaller elements, and the spacing between them is filled with a viscoelastic material. Backing and matching layers are also viscoelastic, and these layers introduce losses. Larger bandwidth leads to larger losses in the transducer, which again cause transducer self-heating. For imaging purposes, a broad-band transducer provides opportunities for imaging at different depths and with different resolutions. Therapy transducers should however produce large outputs, and are dependent upon good efficiency. Efficiency is defined as the ratio between the transmitted acoustic energy and the applied electric energy

$$\eta = \frac{W_{ac}}{W_{el}} \tag{2.39}$$

For therapy purposes, the desired output should be as high as possible, which implies that the losses in the transducer should be as small as possible. This is easier achieved if the transducer operates in a narrow frequency band.

2.3.2 Self-heating and cooling

Transducer self-heating is an important aspect when creating a transducer for treatment purposes. It is important not to burn the patient or the operator, but it is also important not to burn and destroy the piezoelectric material and thereby destroy the transducer. If layers of viscoelastic materials are used, these materials can delaminate, and create layers of air inside the transducer. Air inside the transducer will cause total reflections which again will destroy the transducer elements. Some energy will always be transformed to heat as the piezoelectric elements start to vibrate. One approach to reduce the self-heating is to reduce the duty cycle. The duty cycle is the percentage of a period the signal is active, i.e. the pulse length, T_p relative to the pulse repetition time T_r;

$$DC = \frac{T_p}{T_r} \tag{2.40}$$

By reducing the duty cycle, the transducer will be inactive between each transmitted pulse, which enables heat to dissipate.

2.3.3 Aperture size and shape

Transducers are available in all shapes and sizes, from single-element transducers to matrix arrays with 3D imaging capabilities. In general, transducer apertures are either circular or rectangular. Circular apertures normally consist of one or a few elements, while rectangular transducers normally consist of arrays of smaller elements. The transducer surface can also be flat or curved in order to create focusing as discussed in section 2.2.3.

Circular apertures must have the same focus in elevation and azimuth, while these can be different for rectangular apertures. With regards to beam steering, rectangular arrays allow for electrical beam steering in azimuth, and sometimes also in elevation, direction. In order to steer the beam in one direction, there must be several small elements in that direction in the transducer. If one wants to steer in two direction, a matrix array is needed. Electronic beam steering is fast and easy, however, as mentioned in section 2.3.1, slicing of elements introduces viscoelastic materials which lead to losses in the transducer. Circular apertures cannot be steered electronically, they must be mechanically moved. For imaging purposes, different types of rectangular arrays are widely used. For treatment purposes, there is no definite truth about the best transducer aperture shape. Off-the-shelf transducers designed for high-output purposes are, however, mostly circular, single-element transducers. Another important consideration is the aperture size and its focus. As both the focal length and width are dependent on the F-number (see equation (2.14)), this ratio is crucial in order to design an efficient UMDD scheme.

Chapter 3

Experiment design

There are several considerations that need to be done when designing an animal experiment in order to investigate the effect of ultrasound on drug delivery from nanoparticles to solid tumors. These considerations involve choosing an appropriate transducer, design of an efficient scanning pattern and an efficient and accurate physical set-up of the experiment.

3.1 Physical limitations

The transducer output is limited by the applied input voltage, V_{tt} and the transducer efficiency. The applied input voltage is in turn limited by the available voltage generator and amplifier. In order to generate a high intensity output, one is therefore dependent upon a voltage generator and amplifier which enable the maximum input the transducer can handle.

The average electrical input power delivered to the transducer is

$$P_{el} = V_{tt,rms}^2 \,\mathrm{Re}\left\{\frac{1}{Z_{el}}\right\} DC \tag{3.1}$$

where Z_{el} is the internal electrical impedance in the transducer and DC the duty cycle. $V_{tt,rms}$ is the average input voltage;

$$V_{tt,rms} = \frac{\sqrt{2}}{2} V_{tt} \tag{3.2}$$

The real part of the admittance, $\mathrm{Re}\{\frac{1}{Z_{el}}\}$, can be written as

$$\mathrm{Re}\left\{\frac{1}{Z_{el}}\right\} = \mathrm{Re}\left\{\frac{Z_{el}^*}{Z_{el}Z_{el}^*}\right\} = \frac{|Z_{el}|cos(\phi)}{|Z_{el}|^2} = \frac{cos(\phi)}{|Z_{el}|} \tag{3.3}$$

where ϕ is the impedance phase angle. By combination of equations (3.1)-(3.3), the electrical input power can be expressed as

$$P_{el} = \frac{\sqrt{2}V_{tt}^2 cos(\phi)}{2|Z_{el}|} \cdot DC \tag{3.4}$$

The electrical impedance can easily be measured by an impedancemeter, when frequency-dependent impedance curves are not provided by the transducer manufacturer. Most manufacturers recommend the electrical input power to be lower than a certain threshold, in order not to destroy the transducer by self-heating. For example, Olympus recommends that the average power dissipation to their immersion transducers should not exceed 125 mW [33]. When such a limit is provided, one can choose an available input voltage, and then calculate the maximum duty cycle as

$$DC_{max} = \frac{2|Z_{el}|P_{el,max}}{\sqrt{2}V_{tt}^2 cos(\phi)} \tag{3.5}$$

It is important to recognize that some parameters are bounded by the transducer choice, while others are possible to adjust. The ideal transducer has high efficiency, generates high pressures and tolerates large duty cycles. The duty cycle is important as the desired output not only is a large radiation force, but also a large impulse. This is illustrated in figure 3.1.

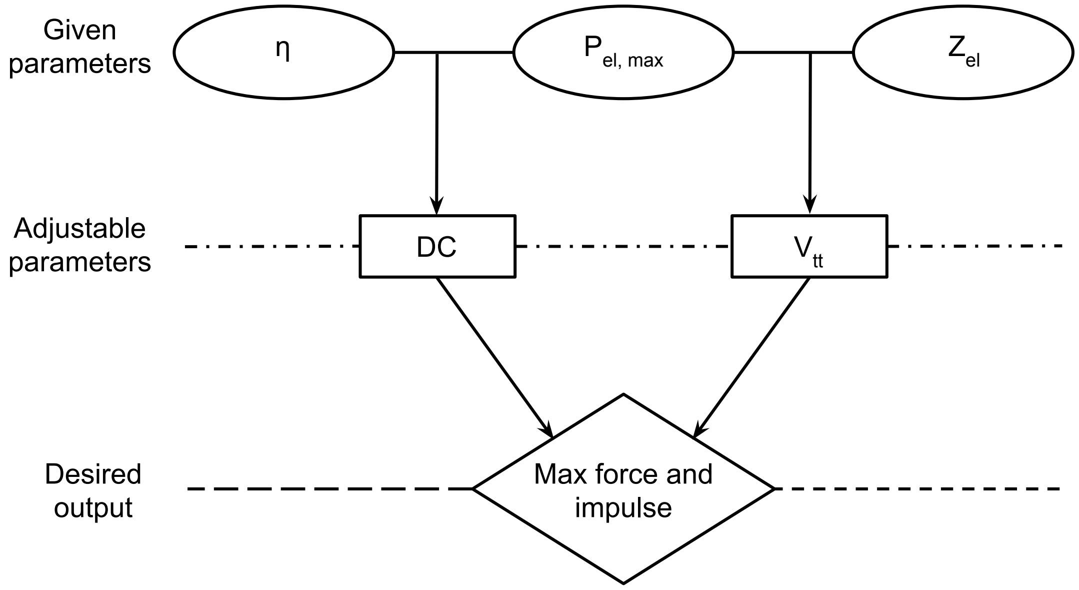

FIGURE 3.1: Transducer parameters governing output for radiation force and impulse.

3.2 Scanning strategy

In addition to determine the maximal output power and duty cycle, the transducer determines the beam profile and thereby also the size and shape of the focal area. This greatly impacts the scanning strategy when conducting an animal experiment.

3.2.1 Tumor placement

As mentioned in section 2.2.3, the transmitted sound field from an ultrasound transducer will consist of areas of constructive and destructive interference. The focal area is the area where the highest pressures and intensities occur. In order to maximize the radiation force, it would therefore be reasonable to place the tumor in the focal zone. However, the area of the focal zone is dependent upon the F-number and wavelength. If the transducer has a high center frequency, or if it is strongly focused, the focal area will be small. A sub-millimetre focal area can be hard to detect in microscopy analysis. In order to irradiate an area which is possible to detect in microscopy analysis, the tumor can be placed in the front or in the back of the focal area, where the beam is wider, but has a lower intensity. It is then important not to place the tumor in destructive interference zones.

3.2.2 Scanning area

When designing an animal trial for treatment purposes, the aim is not necessarily to cure the animal. In an UMDD experiment, it is of higher importance to verify that one is able to move drug carriers from the capillary flow and into the interstitium. The tumor vasculature lies in the peripheral parts of the tumor, it is therefore important to prove that the drug carriers are moved towards the central tumor region after ultrasonic treatment. If the aim was to cure the animal, the whole tumor would need to be irradiated by ultrasound waves. However, for the proof of concept, it is necessary to scan an area which is detectable by microscopy analysis. As mentioned in the above section, the focal zone is potentially small. By placing the tumor in front or back of the focal zone, one gains a larger irradiated area, but looses intensity and thereby applied force. An alternative to this is to scan a wider area by moving the beams. As mention in section 2.3.3, rectangular array transducers often provide electronic beam steering in azimuth, and sometimes also in elevation direction. However, since most commercial therapy transducers are circular single-element transducers, they must be manually moved in order to move the beam and scan an area.

Movement of the ultrasound beam also provides opportunities to avoid tissue heating. If only one spot is treated, heat will accumulate in that area over time. Several beams in different spots will distribute the heat generation. By clever selection of a scanning pattern, one can avoid the heat to accumulate in small volumes over time. A linear scanning pattern will gradually accumulate heat along the scanning line. However, if one chose a pattern where no points in close proximity to each other are scanned following each other, the heat generated at one location will have time to diffuse before an adjacent area is insonified.

As seen from equations (2.14), the length of the focal zone is larger than the width. In order to avoid scanning also in the z-direction, one can chose a frequency and F-number which gives a focal length that covers the tumor in axial direction. However, attenuation of the wave in tissue will lead to reduced intensities in the back of the tumor. Axial scanning will also suffer from attenuation losses, and the generated forces will be smaller in the distal than proximal tumor periphery.

3.2.3 Scanning time

The aim of an experiment to verify the impact of radiation force in UMDD is to create both as large force as possible, but also as large impulse as possible. Impulse is the integral of the applied force over time

$$J = \int F dt \tag{3.6}$$

If the ECM is thixotropic or requires a force above a certain threshold to move the particles, the particle velocity can be modelled as

$$\vec{u} = \mu Pos(F_r - F_0) \tag{3.7}$$

where μ is the friction coefficient of the surrounding tissue, F_r is the URF and F_0 is the threshold which must be overcome in order to initiate particle movement. $Pos(F_r - F_0)$ is the difference between these forces when the URF is larger than the threshold. If the ECM is thixotropic, the matrix will be less viscous when a movement is initiated, and the forces needed to continue the movement might be smaller than the force needed to initiate it. If one only assumes that a threshold is needed to be overcome, the length of the particle movement will be

$$l = \int \vec{u} dt = \mu \int Pos(F_r - F_0) dt \tag{3.8}$$

This implies that one also aims to maximize the efficient scanning time. The maximum scanning time is limited by the half life of the nanoparticle drug carriers.

Over time these carriers will degrade, and in order to reach the desired effect, one should therefore aim to treat the tumor when a significant fraction of the carriers still circulate, i.e. within the half life of the nanoparticles. The maximum efficient scanning time is limited by the duty cycle. If the half life of the particles is T_{hl}, the maximum efficient scanning time will be

$$T_{eff,max} = T_{hl} \cdot DC \tag{3.9}$$

This is the efficient total scanning time over all scanned areas. If more areas are scanned by moving the ultrasound beam, the total efficient scanning time per beam is the total efficient scanning time divided by the number of beams, N.

$$T_{eff,beam} = \frac{T_{eff,max}}{N} \tag{3.10}$$

It is important to notice that with such a scanning pattern the applied force is the same per area, but the impulse per area will be reduced.

Another aspect to consider is the pulse length. Ideally one wants to apply a force to the same particle several times. In order to do so, one must ensure that the pulse repetition frequency is high enough, so that the particle will not move out of the beam between two pulses. The particle movement follows the blood flow, which for tumor capillaries is approximately $40 - 350\,\mu\text{m/s}$ [34]. The distance a particle moves between two following pulses is

$$d = v_b T_r \tag{3.11}$$

where v_b is the blood velocity and T_r the pulse repetition time. This is given by

$$T_r = \frac{T_p}{DC} \tag{3.12}$$

where T_p is the pulse length. If the aim is to hit the same nanoparticle at least twice, the maximum distance it can move between two pulses is the distance corresponding to the smallest beam width. The beam is most narrow in the focal zone, i.e

$$d = v_b T_r = v_b \frac{T_p}{DC} \leq D_f = \lambda F_\# \tag{3.13}$$

This means that the pulse length is limited by

$$T_p \leq \frac{\lambda F_\# DC}{v_{b,max}} \tag{3.14}$$

A longer pulse length enables the transducer to operate in a narrower frequency band. The piezoelectric elements will then vibrate close to their resonance frequency, which in most cases lead to higher efficiency. On the other hand, it is shown that short pulses and high pulse repetition frequency(PRF) creates larger streaming of microbubbles due to URF than long pulses and low PRF [35]. This might be due to resonance in the bubbles, and it is not known whether this effect can be observed with nanoparticles. If this is valid also for nanoparticles, determining the pulse length can be a trade-off between transducer bandwidth and generated particle streaming.

3.2.4 Tumor sectioning and analysis

As mentioned in section 3.2.1, the scanned area must be large enough to detect in microscopy analysis. In order to investigate the results of an *in vivo* experiment, confocal microscopy is used to analyse tumor slices. The nanoparticles are labelled with fluorescent dyes which are detectable in a confocal microscope. By staining the capillaries in a different color, one is able to detect the amount of drug carriers which has left the vessels, and how far they have moved. There are two main strategies to detect this movement:

- The tumor can be sliced horizontally. By knowing where the slices are taken, one can calculate how many particles which have moved into that depth.
- The tumor can be sliced vertically. Stained blood vessels and particle movement will than be available within the same slice, but only in the areas which are covered by the ultrasound beam.

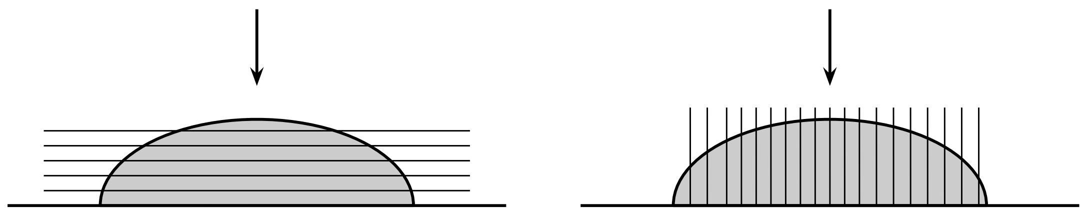

FIGURE 3.2: Possibilities for tumor sectioning. Horizontal slicing to the left, vertical slicing to the right. The arrows indicate the direction of the ultrasound beam.

The two strategies are illustrated in figure 3.2. Both strategies require that one knows where the tumor is scanned. By only scanning a part of the tumor, the other parts can be used as control slices. One would assume more signal from particles in areas which are scanned than those that are not treated by ultrasound.

3.3 Propagation through water

In order to obtain wave distortion and higher frequency components, it is desirable that the wave first propagates through a medium with low attenuation, like water. This will cause larger forces as the high frequency components are absorbed when the wave reaches the tissue. There are several approaches to how this can be done physically. When deciding on a physical set-up, it is important to keep in mind that an acoustic coupling between the transducer and the tumor must be preserved.

In order to ensure good acoustic coupling between the tumor and the transducer, the easiest way would be to immerse both the tumor and the transducer in water. This was done by Eggen et al. [2], as seen in figure 3.3. This experiment was conducted with transducers with low frequencies and relatively large apertures, so that the entire tumor was covered by the ultrasound beam in the focal zone. This type of set-up is not necessarily well suited for smaller transducers and larger frequencies, where mechanical movement of the probe is necessary in order to insonify the desired parts of the tumor. Mechanical movement of the probe does not allow for the transducer to be mounted in the bottom of a water tank.

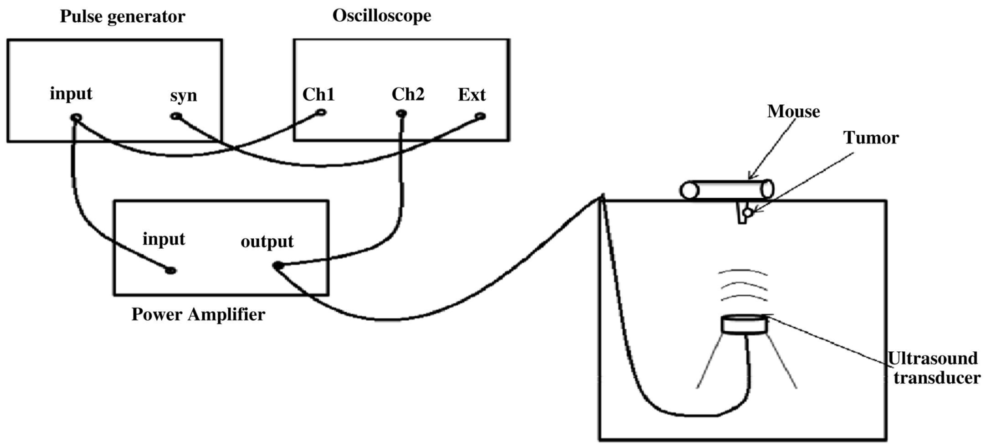

FIGURE 3.3: Radiation force experiment with both transducer and tumor immersed in water [2].

Alternatively, one can move the mouse, rather than the transducer, in order to allow a fixed transducer in the bottom. Another approach can be to mount the transducer to a scanning robot inside the water tank. However, movement of the transducer within the water tank may cause air bubbles in the water, which may lead to reflections of the beam and reduced forces.

Instead of having the transducer at the bottom of the tank and the mouse on the top, one can have the mouse at the bottom and the transducer at the top. This was done by Tung et al. [36], where the mouse was carefully placed underneath a water container as illustrated in figure 3.4. In such a set-up, it is of high importance that the acoustic coupling between the animal and the transducer is preserved. The membrane which separates the water and the mouse should have similar acoustic impedance to water or tissue, in order not to create another reflection interface where energy is lost. It should also be thin, ideally the thickness should be $d = \frac{\lambda}{2}n$, where n is an integer, in order to eliminate reflections.

Reflections from the back of the tumor are also important to consider. Bones in the body are strong reflectors, and so is air. One must therefore carefully select the angle of insonation and place acoustic absorbers in the back of the tumor. If there is bone or air behind the tumor, the wave will be totally reflected into the body, causing a radiation force to act in the opposite direction. The effect

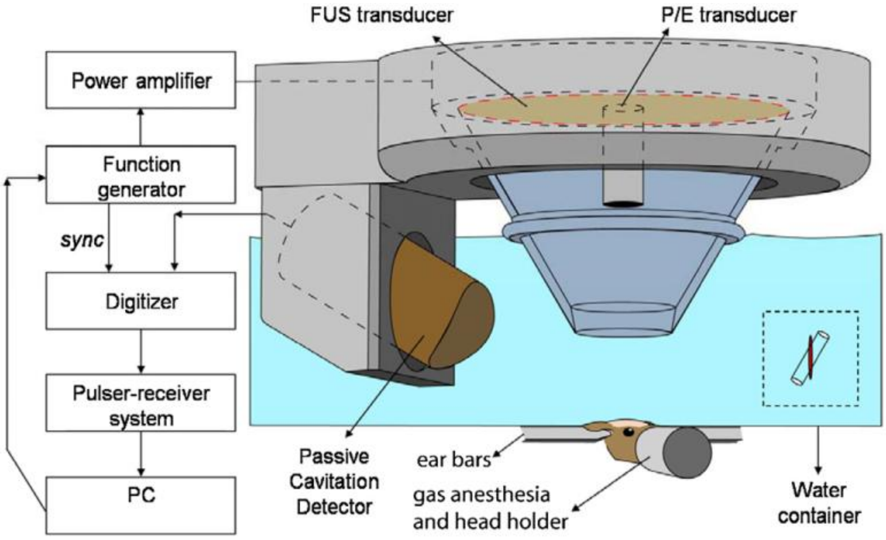

FIGURE 3.4: Ultrasound induced cavitation experiment with the mouse placed underneath the water container [36].

of this force may reduce the effect of the initial radiation force, as it pushes the nanoparticles back in the opposite direction.

Chapter 4

Simulations

In order to design the best possible ultrasound radiation force experiment, it is important to be able to simulate the output from different transducers. This chapter presents different simulations in order to illustrate the output from an Olympus i8-0518-P-SU single element immersion transducer with 60 mm focal length. Since nonlinear wave propagation generates higher harmonics for each depth step iteration, a raised cosine low-pass filter is applied to the field in each depth in order to keep the frequency components of the propagating wave within half the sampling frequency. This filter removes some small contributions from higher harmonics, making the simulations conservative regarding the maximum pressure and URF which is possible to generate.

4.1 Field simulations

As discussed in section 2.2.3, the sound field from an ultrasound transducer can be focused and diffracted. Diffraction pattern is of interest in URF applications, since areas of destructive interference will produce zero or very small radiation forces. Regions of interest should therefore be placed in areas where the sound field has large intensities.

Figures 4.1 - 4.3 illustrate the acoustic field resulting from three different apertures. The beams are all focused in 60 mm and have a center frequency of 5 MHz. The sound waves travel through 55 mm water, before they reach tissue. The simulation parameters for the three simulations are listed in table 4.1

TABLE 4.1: Simulation parameters for field simulations

Simulation parameters	
Center frequency	5 MHz
Aperture	Circular
Aperture width	10, 19 and 29 mm
Pulse length	1 µs
Focus	60 mm
Water propagation	55 mm
Initial pressure	200 kPa

Figure 4.1 shows the sound field generated by a circular transducer with 10mm aperture diamter. The corresponding F-number is $F_{\#} = 6$. This is a relatively large F-number, and the focusing is weak. Two areas of destructive interference can clearly be seen on the beam axis at $z \approx 15$ mm and $z \approx 25$ mm.The focal zone is stretched and wide. It can also be noted that the maximal pressure is relatively small, due to the weak focusing.

Figure 4.2 shows the acoustic output from a 19 mm wide circular aperture, focused in 60 mm. From this simulation, one can clearly recognize the shape of the beam illustrated in figure 2.5. The F-number is $F_{\#} \approx 3$, and it can be seen that the focusing results in higher pressures in the focal zone. Areas of destructive interference can in this figure also be seen on the beam axis. Due to the lower F-number, both the length and width of the focal zone are smaller than in the field generated by a smaller aperture.

Figure 4.3 illustrates a highly focused acoustic field resulting from a transducer with 29 mm aperture width. The corresponding F-number is $F_{\#} \approx 2$, which

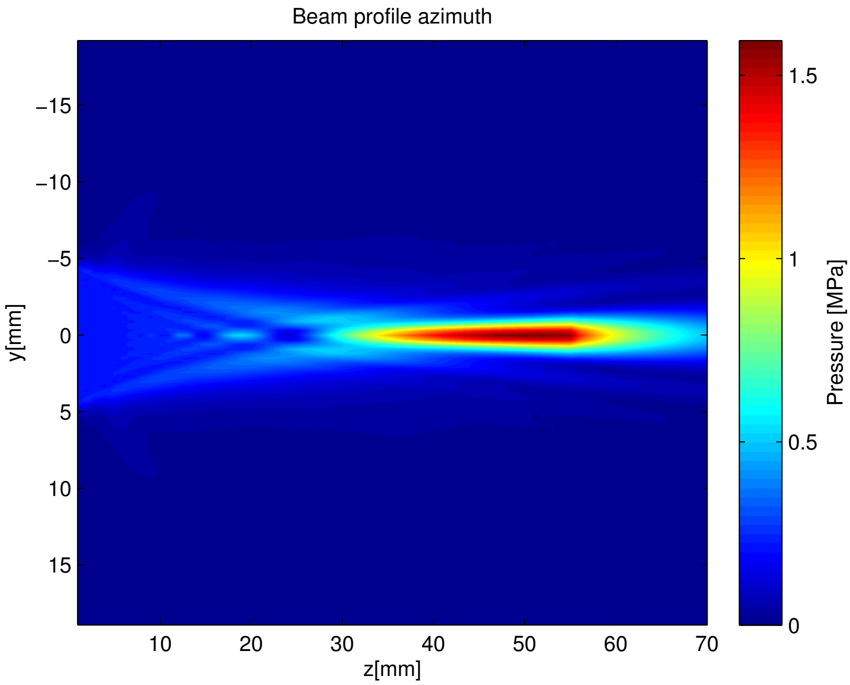

FIGURE 4.1: Beam profile simulated with 10 mm transducer aperture. Center frequency is 5 MHz and the focus is 60 mm. The wave propagates 55 mm in water before it reaches the tissue.

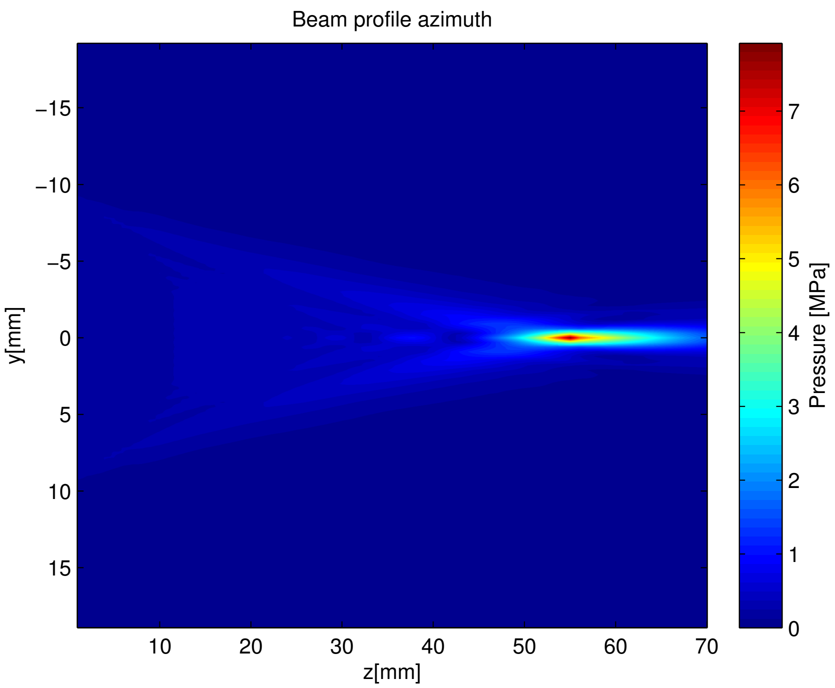

FIGURE 4.2: Beam profile simulated with 19 mm transducer aperture. Center frequency is 5 MHz and the focus is 60 mm. The wave propagates 55 mm in water before it reaches the tissue.

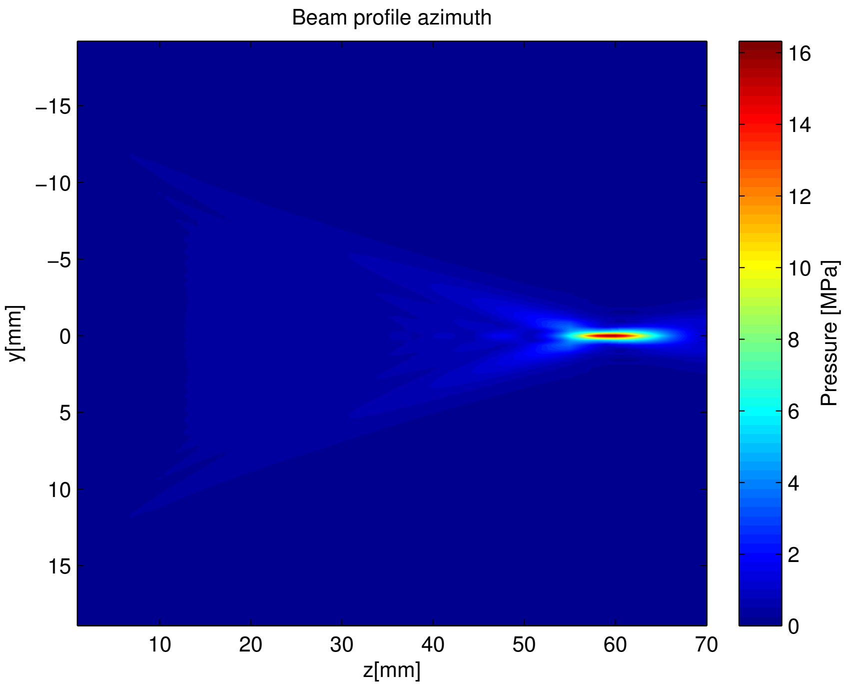

FIGURE 4.3: Beam profile simulated with 29 mm transducer aperture. Center frequency is 5 MHz and the focus is 60 mm. The wave propagates 55 mm in water before it reaches the tissue.

generates high pressures in a narrow focal zone. The pressures shown in the field simulations are the peak positive pressures, as they generate the largest intensities and therefore are of most interest in an ultrasound radiation force context.

4.1.1 Rectangular aperture

Rectangular apertures are common in medical imaging applications. They can however also be used for treatment purposes. Figure 4.4 and 4.5 show the beam profiles in azimuth and elevation resulting from a rectangular aperture. The simulation parameters used in this simulation are given in table 4.2.

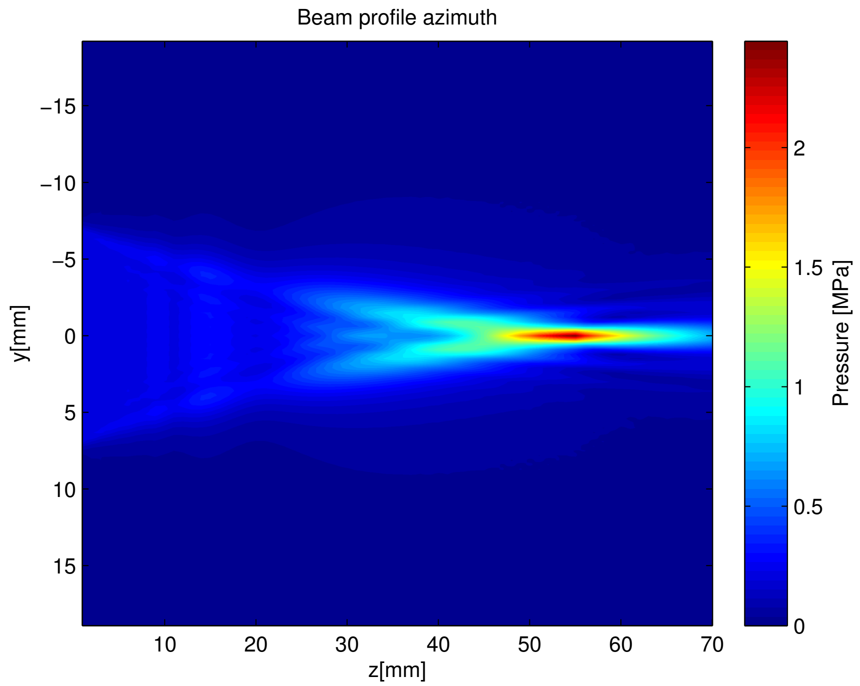

FIGURE 4.4: Azimuth beam profile simulated with a rectangular aperture. Center frequency is 5 MHz and the focus is 60 mm. The wave propagates 55 mm in water before it reaches the tissue.

TABLE 4.2: Simulation parameters for rectangular aperture

Simulation parameters	
Center frequency	5 MHz
Aperture azimuth	15 mm
Aperture elevation	8 mm
Pulse length	1 µs
Focus azimuth	60 mm
Focus elevation	60 mm
Water propagation	55 mm
Initial pressure	200 kPa

Both azimuth and elevation focus is in 60 mm. This corresponds to an F-number in azimuth of $F_{\#,azi} = 4$ and in elevation $F_{\#,elev} = 7.5$. The different F-numbers lead to very different beam profiles and pressure distributions in elevation and

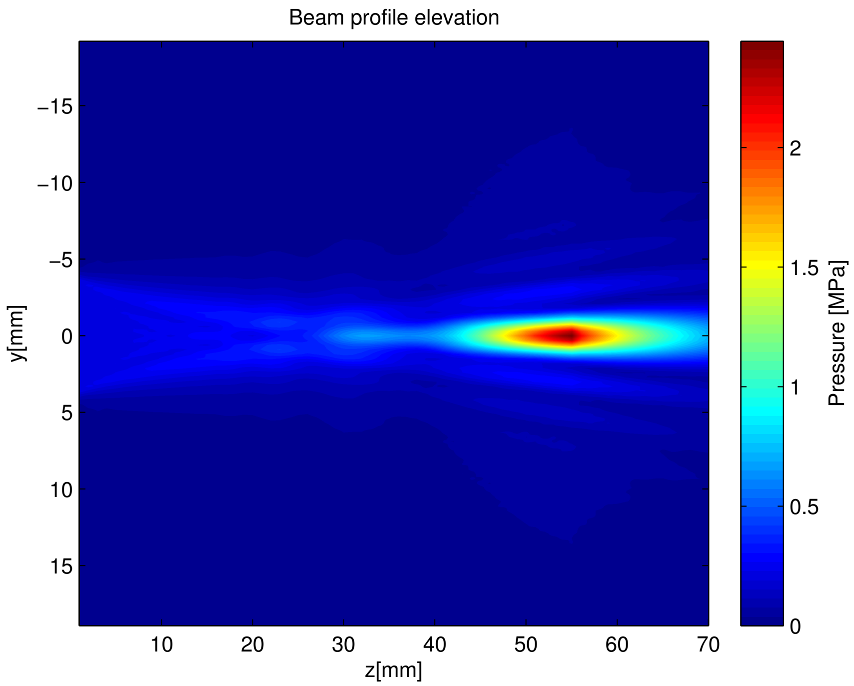

FIGURE 4.5: Elevation beam profile simulated with rectangular aperture. Center frequency is 5 MHz and the focus is 60 mm. The wave propagates 55 mm in water before it reaches the tissue.

azimuth. The interference pattern is fundamentally different from the circular apertures simulated in the above section. Due to the rectangular aperture, less areas of destructive interference are created, and no zero-points can be seen on the axis. In elevation the rectangular aperture is very weakly focused. This can be seen in the resulting beam profile, where the focal zone is long and wide. Another interesting phenomena is the side lobes generated in elevation. Since the beam is weakly focused, a large amount of the energy is directed in angles different from the propagating direction. These waves interfere and form side lobes symmetrically around the beam axis. The weakly focused elevation aperture leads to a more evenly distributed pressure profile also in azimuth. The energy is not directed similarly in azimuth and elevation, resulting in less constructive interference and lower generated pressures.

4.2 Ultrasound radiation force

Simulation of the URF output is valuable when planning an URF experiment. Simulation of the generated force on the axis as well as the distribution of force throughout the region of interest can be helpful in order to choose an appropriate transducer and design the physical set-up of the experiment.

4.2.1 Frequency dependence

There are two main effects the choice of frequency has on the generated URF. These are

1. The extinction cross section increases with increasing frequency.
2. The non-linear distortion of the waveform generates higher harmonic frequency components in the focal zone, which lead larger forces.

Since these effects are non-linear, it is interesting to investigate to which extent URF is dependent upon the center frequency. Figure 4.6 illustrates a simulation of URF generated on the beam axis with varying center frequency. The parameters used in the simulation are given in table 4.3.

TABLE 4.3: Simulation parameters for URF frequency dependency

Simulation parameters	
Center frequency	Varying
Aperture	Circular
Aperture width	29 mm
Pulse length	1 µs
Focus	60 mm
Water propagation	55 mm
Initial pressure	200 kPa

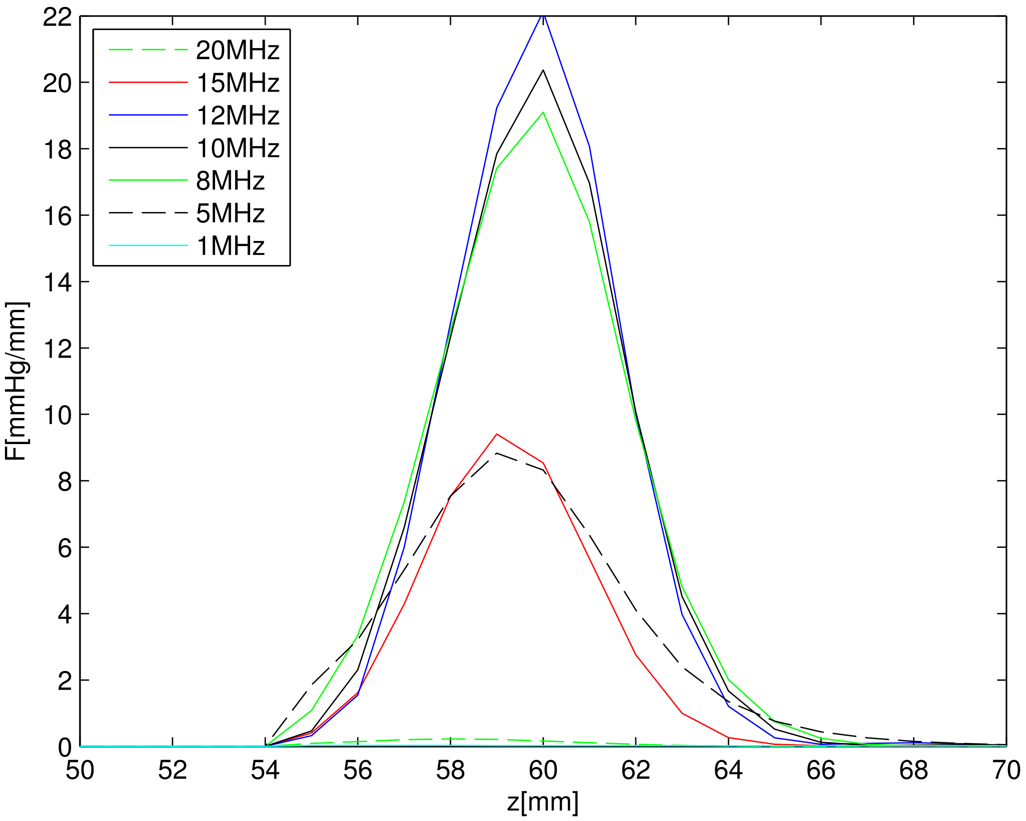

FIGURE 4.6: Frequency dependency of ultrasound radiation force distribution for the parameters given in table 4.3.

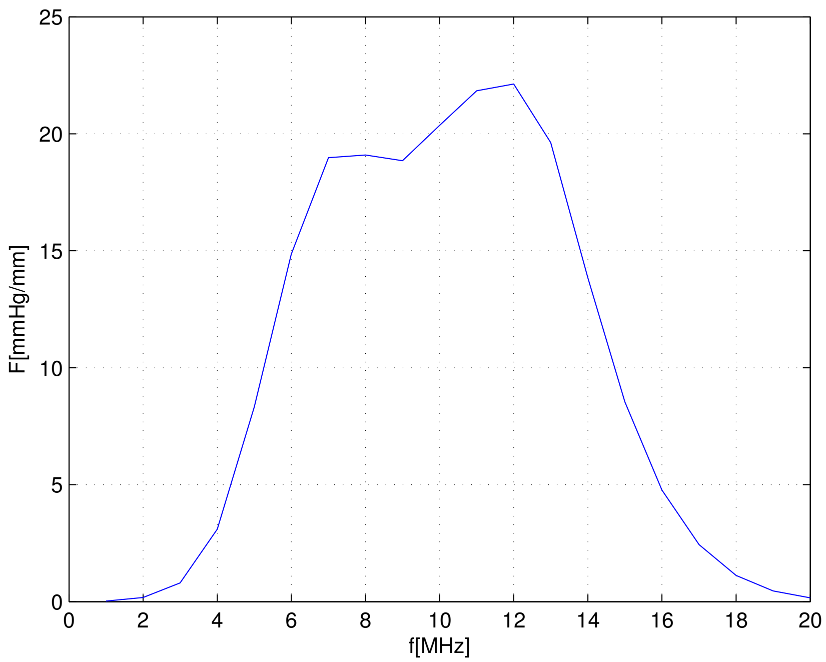

FIGURE 4.7: Frequency dependency of ultrasound radiation force in focus (60 mm) for the parameters given in table 4.3.

As seen from these simulations, the radiation force is at largest for center frequencies of $8 - 13\,\mathrm{MHz}$. This is due to the fact that extinction cross section increases with increasing frequency. From equation (2.36) it can be seen that the frequency for maximum intensity drops with increasing depth, as the extinction cross section will reduce the intensity. For frequencies up to $\sim 13\,\mathrm{MHz}$, the increasing extinction cross section produces a larger force. For frequencies larger than $\sim 13\,\mathrm{MHz}$, the increasing extinction cross section attenuates so much of the wave intensity, that the product results in a decreasing force for increasing frequencies.

4.2.2 Effect of non-linearities

As seen from figures 2.2 and 2.3 in chapter 2, non-linearities greatly impact the waveform and frequency components of the propagating wave, and thereby also the generated peak pressures. URF is proportional both to extinction cross section and intensity and is therefore highly dependent on the non-linear waveform. Energy pumped into higher harmonics will generate a larger extinction cross section, which contributes to a larger generated force.

Figures 4.8 - 4.11 show simulations of ultrasound radiation force generated by simulation parameters in table 4.4. Figures 4.8 and 4.9 are generated by linear simulations, while figures 4.10 and 4.11 are generated by non-linear simulations.

Comparing the linear and the non-linear simulations, one can clearly see that the amplitude of the generated force is approximately four times larger for the non-linear simulation. It is also worth noting that the force field looks different with linear and non-linear simulation. This is due to diffraction of the higher harmonic components in the non-linear simulation. Higher harmonics generate narrower beamwidths and reduced side-lobe levels in the field [37, 38]. The non-linear field is more directed behind the focal point, as higher frequencies are attenuated and more energy is lost in the propagation. This can also be seen from the axial distribution of the force.

Figure 4.9 shows the radiation force generated on the beam axis with a linear simulation. As water is assumed to have no attenuation, no force is generated before the wave reaches the tissue. However, when the wave reaches tissue, the generated force is approximately -1.5 dB lower than the maximum force. The -3 dB limit is approximately in 63 mm. For the non-linear case, as illustrated in figure 4.11, the force generated at the interface between water and tissue is -6.9 dB lower than the maximum force. The -3 dB width is approximately from 57 to 62 mm. This shows that a larger force is distributed in a smaller area when non-linear propagation is assumed.

TABLE 4.4: Simulation parameters for URF simulation

Simulation parameters	
Center frequency	5 MHz
Aperture	Circular
Aperture width	29 mm
Pulse length	1 µs
Focus	60 mm
Water propagation	55 mm
Initial pressure	200 kPa

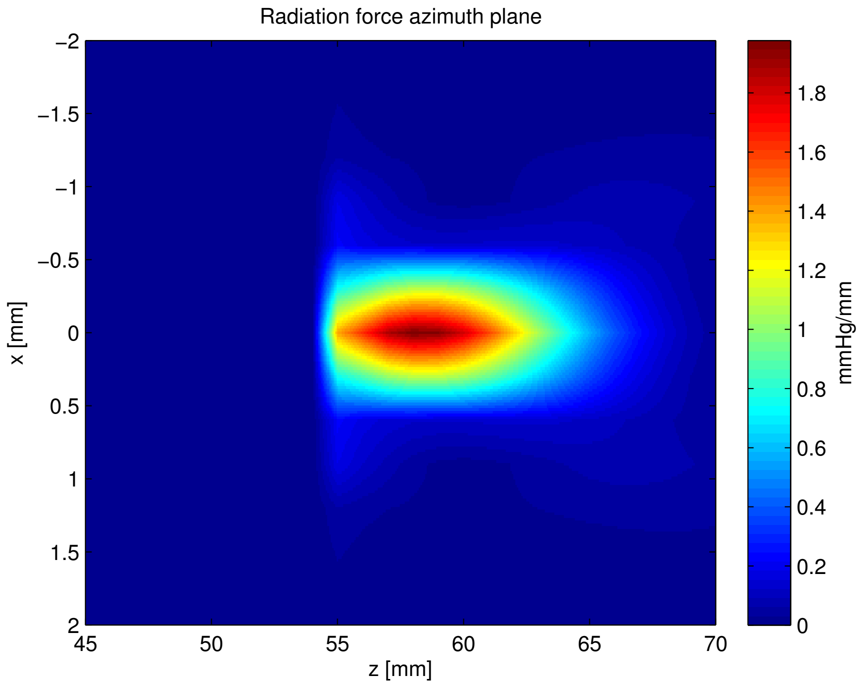

Figure 4.8: Radiation force distribution generated by a linear simulation of the propagating wave. The aperture is 29 mm, center frequency is 5 MHz and the focus is in 60 mm.

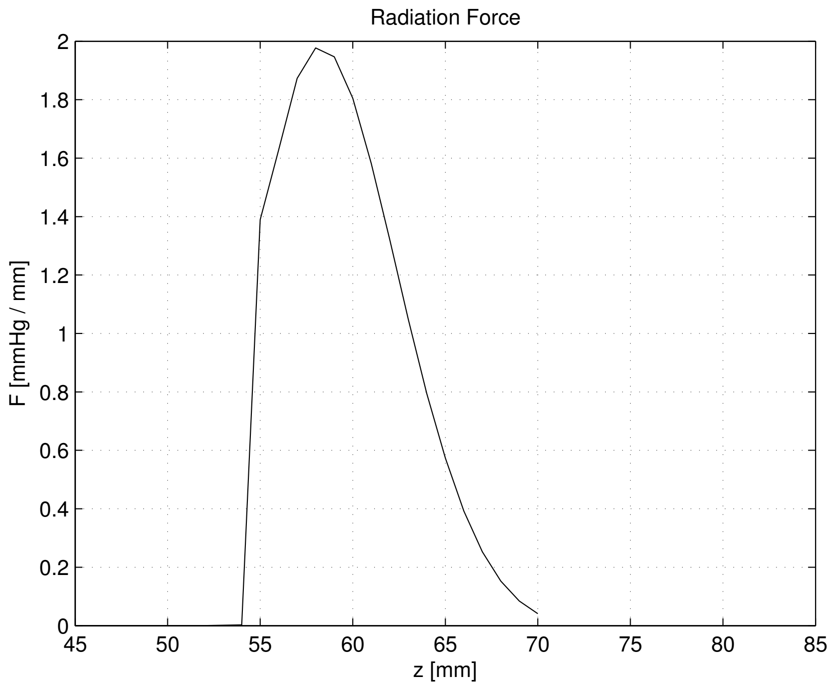

Figure 4.9: Radiation force on the beam axis generated by a linear simulation of the propagating wave. The aperture is 29 mm, center frequency is 5 MHz and the focus is in 60 mm.

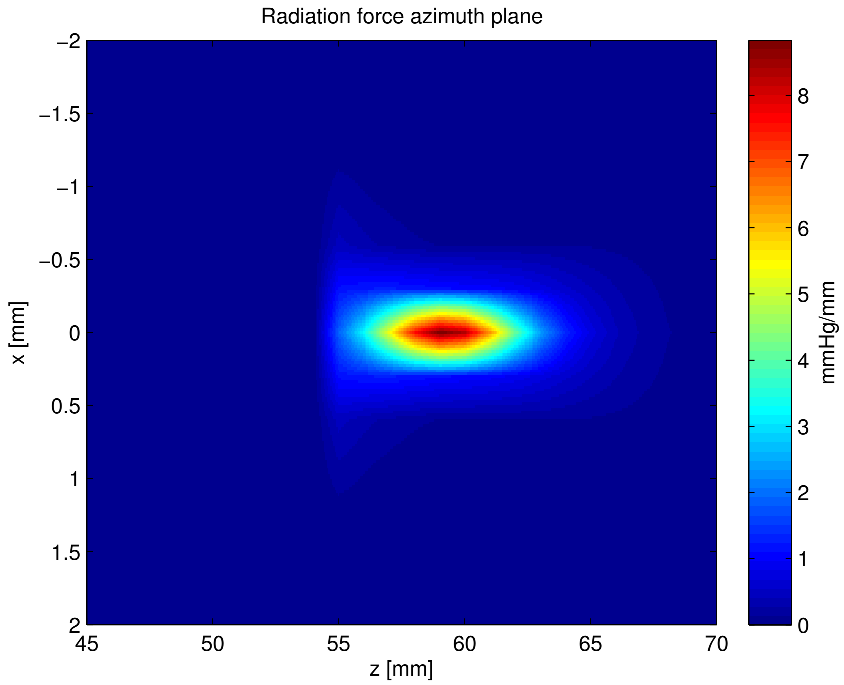

FIGURE 4.10: Radiation force distribution generated by a non-linear simulation of the propagating wave. The aperture is 29 mm, center frequency is 5 MHz and the focus is in 60 mm.

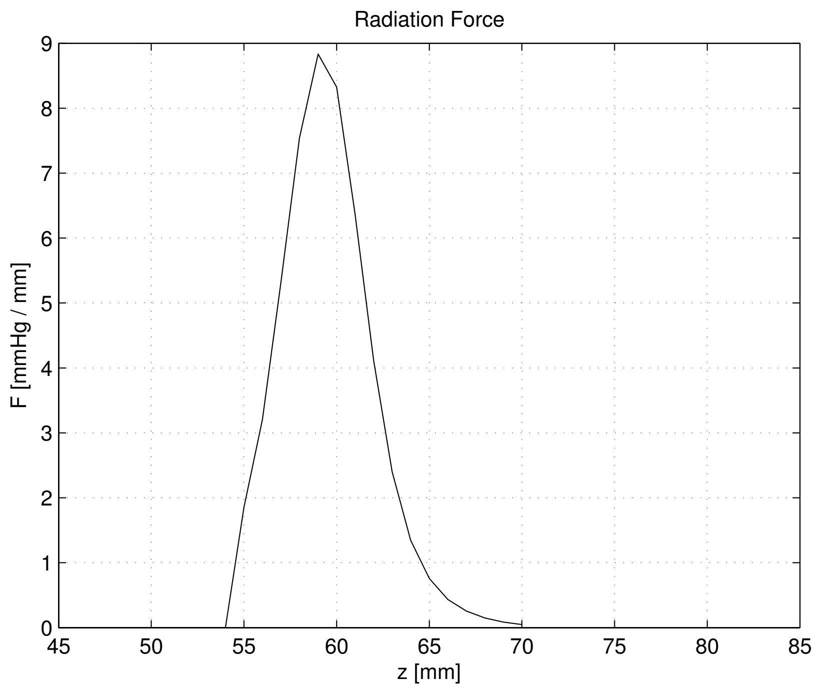

FIGURE 4.11: Radiation force on the beam axis generated by a non-linear simulation of the propagating wave. The aperture is 29 mm, center frequency is 5 MHz and the focus is in 60 mm.

Chapter 5

In vivo experiment

An *in vivo* experiment was conducted in cooperation with Professor Catherina deLange Davies' group at the Department of Physics. Human prostate cancer xenografts were implanted in the back right leg of 28 nude mice. 23 of these mice developed tumors larger than 6 mm in diameter, and could be used in the experiment.

5.1 Transducer

The transducer used in the experiment was an Olympus i8-0518-P-SU single element immersion transducer, with center frequency of 5 MHz. This transducer is from the Olympus HARISONIC "P" series, which is a series of transducers intended to provide high output and penetrating power [33]. The aperture diameter is 29 mm and it is focused in 60 mm. Initially, four different transducers were ordered, in order to chose the best one based on the characterization measurements. Two of these had a center frequency of 10 MHz, and two had a center frequency of 5 MHz. However, due to internal miscommunication within Olympus, the i8-0518-P-SU transducer was the only one which was focused and therefore suitable for the experiment.

Watertank measurements determined the efficiency of the transducer to be $\eta \approx 6{-}10\,\%$. Olympus recommends the electrical input power to be limited to 125 mW. However, temperature and impedance measurements indicated that the transducer could be driven at an electrical input power of $P_{el} = 2\,\mathrm{W}$ when immersed in water, without changes in the input impedance or significant heat generation. The transducer specifications are listed in table 5.1

Table 5.1: Transducer specifications for *in vivo* experiment

Transducer specifications	
Center frequency	5 MHz
Aperture	Circular
Aperture size	29 mm
Focus	60 mm
Efficiency	6-10 %
$P_{el,max}$	2 W
$\lvert Z_{el}\rvert$	48 Ω
ϕ_{el}	21°

The transducer F-number is $F_{\#} \approx 2$, which gives the corresponding focal length and width;

$$D_f \approx 0.6\,\mathrm{mm} \qquad \text{and} \qquad L_f \approx 5\,\mathrm{mm} \tag{5.1}$$

Since most tumors were wider than they were tall, it was decided not to scan in the z-direction, as the focal length covers almost the entire tumor.

The available power amplifier was a ENI 2100L 55 dB amplifier (ENI, Rochester, NY, USA), however, its behaviour was not entirely linear. A 1 V peak to peak input voltage was amplified to 360 V by the amplifier, but gradually reduced to 340 V during 15-20 minutes of scanning. With respect to the highest generated peak to peak voltage, the maximal duty cycle was calculated to be $DC_{max} = 0.15\%$. The pulse length was chosen to be 5 cycles, i.e. 1 µs. This gave a pulse repetition time of $T_r = 666\,\mu\mathrm{s}$, and the corresponding PRF is 1.5 kHz.

5.2 Practical set-up

In order to create a large enough scanning area to be detected in a microscope, a 3 by 3 point scanning pattern in the lateral plane was decided, as illustrated in figure 5.1. The distance between each point in the pattern corresponds to the focal width, i.e. 0.6 mm. The robot which was used did not allow for a more sophisticated scanning pattern. Therefore, a test scan was done in a piece of chicken meat with a thermocouple to monitor any temperature change before the *in vivo* experiment was conducted. The thermocouple did not record any significant changes in temperature, and it was therefore assumed that a linear scanning strategy would not lead to any significant heat generation in the mice.

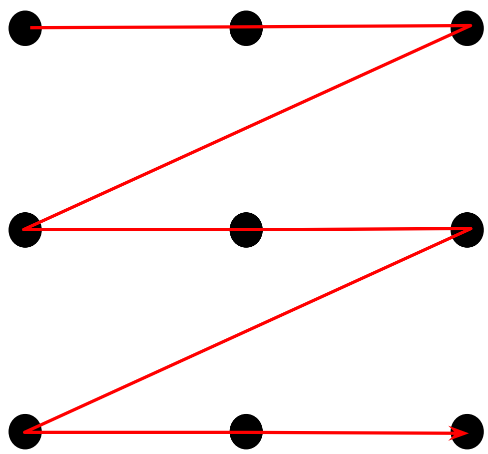

FIGURE 5.1: Scanning pattern for *in vivo* experiment

5.2.1 Experiment groups

The nanoparticles used in the experiment were Silica particles with a diameter of approximately 70 nm. The particle half life in mice was measured to be approximately two hours. The purpose of the experiment was to investigate two different effects:

1. Is URF able to enhance transport of particles through the capillary walls in solid tumors?

2. Is URF able to push particles through the ECM and into central parts of the tumor?

In order to investigate these effects, the mice were divided into two groups:

1. In order to investigate whether URF can enhance transport across the capillary walls, the first group would get ultrasound treatment directly after injection of nanoparticles in the blood. The scan would last for one hour, to ensure that a large amount of the particles was still circulating when the treatment was conducted.

2. To investigate the effects of URF on particle movement through the ECM, the particles were allowed to circulate for four hours before the treatment was conducted. The amount of particles in the blood would then be small, and one could look at the effects on the particles which had passed the capillary walls due to convection.

Another research question interesting to investigate, was whether or not the ECM has thixotropic properties, and whether force or impulse is of most importance. In order to investigate this, each of the two groups were divided into two subgroups:

1. The first group was exposed to ultrasound generated with the maximum voltage available.

2. The second group was exposed to ultrasound generated with approximately half of the voltage in group one, but the same power.

In addition to these four groups, two control groups were used. These groups were not exposed to ultrasound. The first control group got nanoparticles which were allowed to circulate for one hour and fifteen minutes. The other control group got nanoparticles which were allowed to circulate for four hours. The number of mice in the control groups was limited, but the actual amount of control mice is larger. This is due to the fact that only a small volume of the tumors are insonified, and the rest of the tumor can then serve as control slices. In that way, the mouse in the insonified groups also serve as an internal control. The parameters for each group is given in table 5.2.

TABLE 5.2: Groups in the *in vivo* experiment. The number of mice in the control groups is limited due to the use of non-insonified tumor areas as control slices in the groups which are exposed to ultrasound.

Group	Group 1	Group 2	Group 3	Group 4	Group 5	Group 6
#mice	2	5	5	5	5	1
NP circulation time	4 hours	15 min	4 hours	4 hours	15 min	1h15min
Voltage	-	340 V	340 V	160 V	160 V	-
Input power	-	2 W	2 W	2 W	2 W	-
Duty cycle	-	0.15 %	0.15 %	0.6 %	0.6 %	-
Pulse length	-	1 µs	1 µs	1 µs	1 µs	-
PRF	-	1.5 kHz	1.5 kHz	6 kHz	6 kHz	-
Remark	*control*	-	-	-	-	*control*

5.2.2 Physical set-up

Since a 3 by 3 scanning pattern was used, the transducer had to be able to move in order to scan multiple points. It was therefore concluded that it would be easiest with the water bath on top of the mouse, with some space for the transducer to be moved. A transducer holder was produced and mounted to a stepping robot. The water bath was created by attaching a transparent plastic bag to a circular metal ring so that it was shaped like a cone when it was filled with water. This setup is illustrated in figures 5.2 - 5.4.

The tumor was placed underneath the tip of the water bath cone, to ensure that the transducer was directed towards the tumor. In order to ensure good acoustic coupling, the tumor was covered with ultrasound gel both from above and underneath. The mouse was resting on a surgical mat on top of a heating mat, to keep

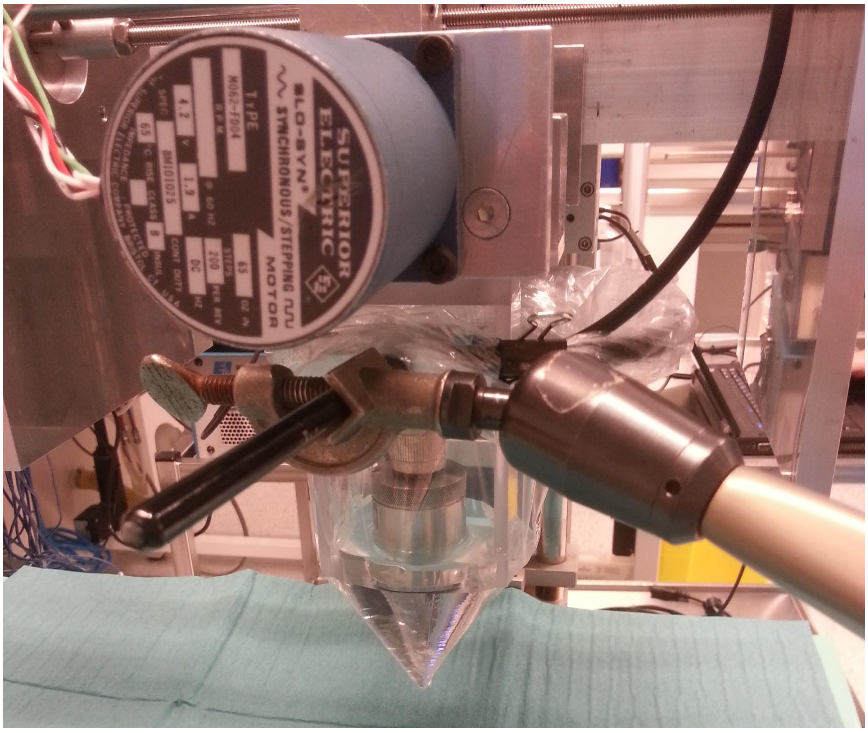

FIGURE 5.2: Water bath and transducer position in the *in vivo* experiment. The water bath is a cone shaped transparent plastic bag, and the transducer is directed towards the tip of the cone.

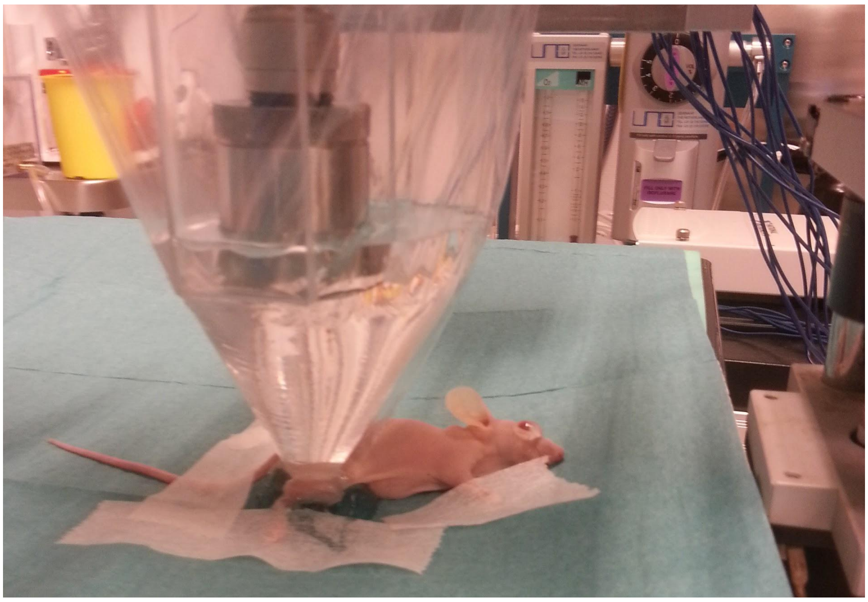

FIGURE 5.3: Positioning of the mouse in the *in vivo* experiment. The tumor is placed underneath the tip of the water bath cone, to ensure that the transducer is directed towards the tumor. The tumor is covered with ultrasound gel in order to ensure good acoustic coupling.

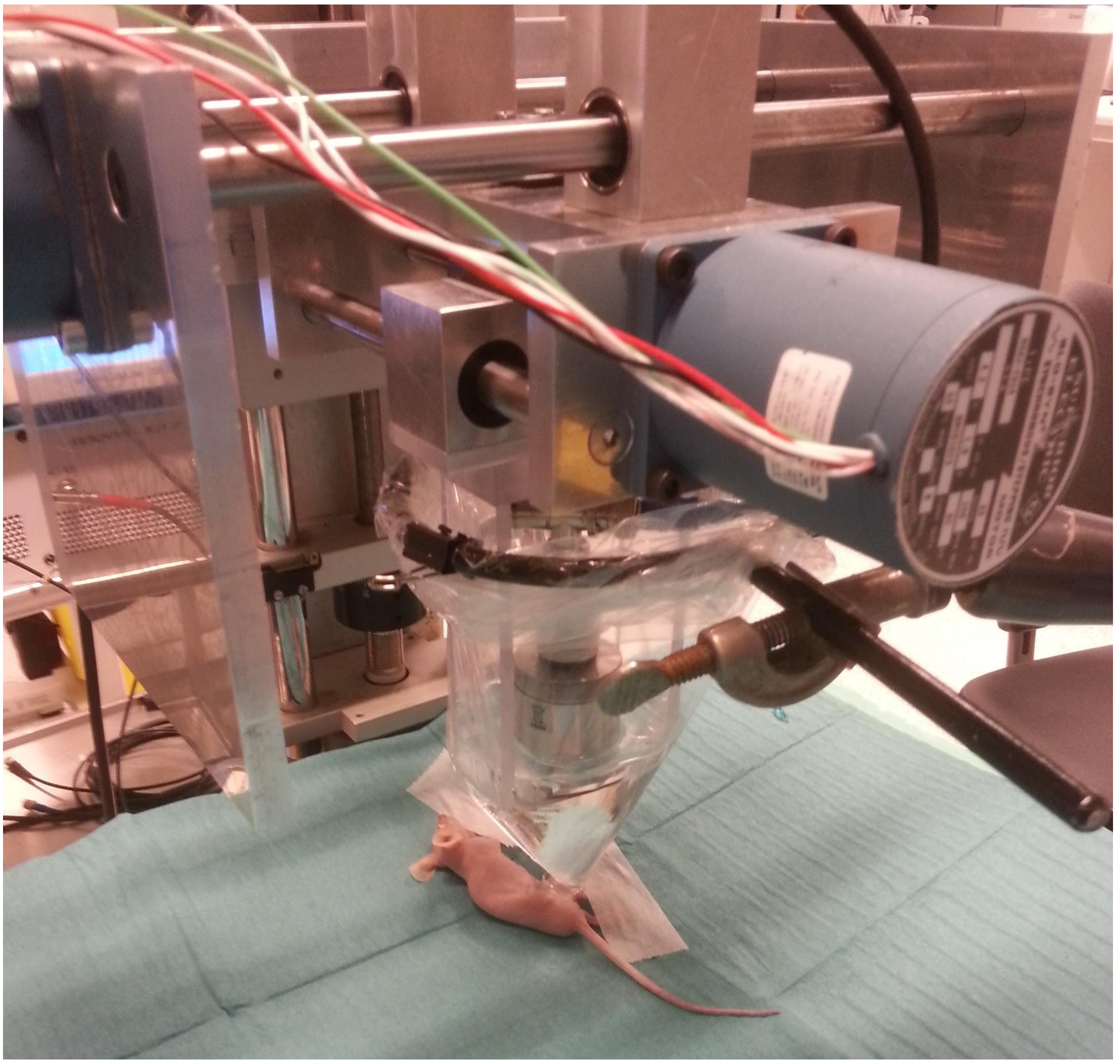

FIGURE 5.4: Entire set-up with stepping motor for the *in vivo* experiment. The water bath is mounted to a separate holder.

the body temperature around 37 °C. Underneath the heating mat, an acoustic absorber was placed in a water bath, in order to avoid reflections which potentially could cause forces acting in the opposite direction.

After treatment, the mouse was euthanized, and the tumor was removed and mounted to a cork plate and frozen. The tumor was mounted to the plate so that sectioning can be done vertically, as illustrated in fig 3.2.

Chapter 6

Discussion

Quality assurance has high importance when an animal experiment should be designed and conducted. Ethical questions rise immediately once animal trials are used to investigate and verify treatment methods. The aim is therefore to design reproducible experiments with as few unknown parameters as possible. This is discussed in the following chapter for an ultrasound radiation force experiment in mice.

6.1 Transducer selection

As mentioned in section 2.3, high intensity ultrasound treatment transducers need to have high efficiency, and be able to produce large acoustic output power. From figure 3.1, the parameters which are given by the transducer are

1. The efficiency, η
2. The maximal electrical input power, $P_{el,max}$
3. The electrical impedance, Z_{el}

All these parameters determine the possible acoustic output power the transducer can generate, and thereby also the force and impulse which are possible to achieve.

Selection of the right transducer therefore greatly impacts the outcome of an ultrasound radiation force experiment. However, only one of the above listed parameters is provided by most manufacturers. The maximum tolerated input power is normally provided in the technical notes from transducer manufacturers. This value is, however, set conservatively low, and is the power limit when the transducer is exited into air, which generates large reflections at the transducer surface. For an ultrasound radiation force set-up where the transducer is loaded with water, it will most likely tolerate a larger input power than the maximum given by the manufacturer. This means that one in practice should investigate how much power the transducer can tolerate, if the maximum limit set by the manufacturer is low.

The efficiency is in most cases not available from the manufacturer. This parameter must therefore also be determined when a transducer is available. Efficiency measurements can be done with hydrophone in a water tank. For a given electrical input power, the generated acoustic output power can be measured by the hydrophone. Based on this, the efficiency can be calculated from equation (2.39).

Electrical impedance might be estimated by the manufacturer, but it must be determined accurately by impedancemeter measurements. Some manufacturers claim to tune all transducers to a given impedance, however, accurate measurements are rarely provided. As most voltage generators have $50\,\Omega$ electrical impedance, the transducer should have an electrical impedance as close as possible to this, with a small phase angle.

In sum, this means that one has to chose a transducer based on more or less unknown parameters. There are, however, possibilities to make qualified estimates of the transducer performance, based on the estimates and descriptions available from the manufacturers. Among others, the intended purpose of the transducer will be described. Therapy transducers will in general have larger efficiency and possibility to generate larger acoustic outputs than imaging transducers. The pulse form and bandwidth are also parameters which are available. Narrowband transducers do often have higher efficiency than broadband transducers.

6.1.1 Frequency

As seen from the simulations in section 4.2.1, the URF is at largest for frequencies between $\sim$ 8 to 13 MHz. In order to gain the highest forces, one should therefore choose a transducer with a center frequency within that frequency band. A narrowband transducer will in most cases give the largest efficiency. In order to cover an area as large as possible, it might be clever to chose a transducer with center frequency around 8 MHz rather than 13 MHz. It is important to bear in mind that animal experiments are conducted to design treatment strategies which later can be applied in humans. One must therefore strive to choose equipment which has potential also in a clinical setting.

As mentioned in section 5.1, four different transducers were ordered in order to choose the best one for the *in vivo* experiment. Initially, the idea was to explore the results *in vivo* with a 10 MHz transducer, as one would expect this to create the largest forces. The 5 MHz transducers were ordered in case the 10 MHz transducers showed poor performance, or alternatively investigate the effect of two different frequencies and compare this to the simulations. It will however be interesting to investigate the results from the 5 MHz transducer. If this transducer is able to generate large enough forces to move the particles through the ECM, larger frequencies might not be needed. In order to investigate this, the mechanical properties of the ECM in tumors should be studied. An estimate of how large forces which are needed to move particles within the ECM would be valuable in order to optimize the selection of transducer center frequency.

6.1.2 Aperture

Ideally, one could imagine a combined treatment and imaging system, which provides electronically beam steering in both azimuth and elevation. The imaging system could then be used to position the tumor correct within the sound field. However, one must overcome several technological barriers before such a system is commercially available. A rectangular aperture provides a beam profile with less destructive interference than a circular aperture does. In that way, a rectangular aperture is more convenient with respect to tumor placement within the sound field. However, commercial transducers which are designed for high intensity ultrasound purposes, are mostly circular single element apertures. These transducers are able to generate large forces, but since a single element only is capable of pulse-echo measurements, positioning the transducer accurately above the tumor is a challenge. A pulse-echo measurement is only capable of determining the time from one echo to the next, and thereby the distance to the scatterer. It is however not possible to know exactly where the wave is reflected, and therefore difficult to be sure that the targeted area lies within the sound field.

6.2 Tumor placement

Placement of the tumor within the sound field is a question which rises in particular when an UMDD scheme is introduced to the clinic. For *in vivo* experiments in mice, the area which needs to be insonified is so small that the tumor can be placed in a narrow focal zone. However, when larger tumors in humans should be treated, a larger area must be covered within the half life of the drug carrying particles. This implies that the sound field must cover a larger area of the tumor and that the transducer must have high efficiency and tolerate large duty cycles.

For an ultrasound radiation force experiment in mice, the area which must be covered is small, and placing the tumor within the focal zone will generate the largest forces. There are, however, very little knowledge about how large force is needed to apply in order to be able to move the particles. One can therefore imagine that this could be investigated further in future *in vivo* experiments. If smaller forces also are sufficient to push the particles across the capillary walls and through the interstitium, the tumor could advantageously be placed in front of the focal area.

In the conducted *in vivo* experiment, the tumor was placed within the focal zone. The transducer was exited with two different voltages, but the same total power for the different groups in the experiment (see table 5.2). The lower voltage generates lower intensities in the focal zone. The results from this experiment must be analysed in order to investigate whether the variation in intensities makes a difference or not. If one is able to detect particle movement also in the groups that got lower intensity treatment, this can be an indication of the importance of maximal impulse rather than maximal force. However, if particle movement is larger in the groups with maximal intensity, this can be an indication of thixotropic properties of the ECM, which create the need for large forces in order to be able to move particles to central tumor areas.

6.3 Practical set-up

As the focal zone was narrow, a scanning strategy was needed in the *in vivo* experiment. It was therefore concluded that a water bath where the transducer could move on top of the mouse was the best solution. The water bath was made from a transparent plastic bag and a metal ring. This was not a robust solution. The metal ring was approximately 14 cm in diameter, and it was difficult to access the transducer surface to remove air bubbles. Positioning the transducer above the tumor was also not a straight forward process. The plastic bag slided slightly on the metal ring, so that the transducer needed to be repositioned between every scan. For reproducibility and quality assurance, a more robust set-up should be constructed.

The mats on which the mouse rests, are also sources of unpredictable behaviour. As mentioned in the previous chapter, the tumor was covered in ultrasound gel both from above and below. However, it was hard to create good acoustic coupling between the gel on top of the surgical mat and the acoustic absorber below the heating mat. The weight of a mouse is around 15 to 20 g, which creates a minimal pressure against the surface of the surgical mat. This allows for air bubbles and cavities to form between the two mats in front of the acoustic absorber. When air was present, this could clearly be seen from pulse-echo measurements as a strong reflector. Future experiments should try to minimize this problem, in order to ensure that the majority of the sound waves propagate in the same direction.

An important aspect is that tumors in the human body are not always close to the skin and easily accessible. Tumors can often be found in internal organs in the body, like prostate, liver and pancreas. This is a challenge in UMDD. As seen from figure 2.4, the sound waves are strongly attenuated as they propagate through tissue. Nonlinear effects accumulate in mediums with low attenuation, but are attenuated in absorbing mediums. One must be able to generate high intensities as well as higher harmonic components in order to generate a significant radiation force. This is one of the main challenges in developing an UMDD scheme which is suitable for clinical use.

Chapter 7

Conclusions

Previous *in vivo* experiments have shown promising results for the use of ultrasound radiation force to enhance transport of macromolecules across the vessel walls in solid tumors. However, the results from the conducted experiment must be analysed in order to gain new knowledge about the mechanisms of ultrasound mediated drug delivery. There are still technological and biological barriers to overcome before ultrasound radiation force can be used in the clinic, and further *in vivo* experiments must be conducted before one can start clinical trials. The importance of increased therapeutic indices for chemotherapeutic drugs is clear, and ultrasound radiation force shows great potential in enhancing this. With development of high-performance ultrasound transducers and scanners, ultrasound mediated drug delivery can be a treatment method for the future.

References

[1] Ahmedin Jemal, Freddie Bray, Melissa M. Center, Jacques Ferlay, Elizabeth Ward, and David Forman. Global cancer statistics. *CA: A Cancer Journal for Clinicians*, 61:69–90, 2011.

[2] Siv Eggen, Mercy Afadzi, Esben A. Nilssen, Solveig Bjærum Haugstad, Bjørn Angelsen, and Catharina de L. Davies. Ultrasound improves the uptake and distribution of liposomal doxorubicin in prostate cancer xenografts. *Ultrasound in Medicine and Biology*, 39:1255–1266, 2013.

[3] Joshua J. Rychak, Alexander L. Klibanov, and John A. Hossack. Acoustic radiation force enhances targeted delivery of ultrasound contrast microbubbles: In vitro verification. *IEEE transactions on ultrasonics, ferroelectrics, and frequency control*, 52:421–433, 2005.

[4] Harvey F. Lodish, Baltimore, Matsudaira, Zipursky, and Berk. *Molecular Cell Biology*. Freeman, W.H. & Company, 4 edition, 1999.

[5] Robert A. Weinberg. How cancer arises. *Scientific American*, pages 62–70, 1996.

[6] Petros Koumoutsakos, Igor Pivkin, and Florian Milde. The fluid mechanics of cancer and its therapy. *Annual Review of Fluid Mechanics*, 45:325–355, 2013.

[7] Douglas Hanahan and Robert A. Weinberg. The hallmarks of cancer. *Cell*, 100:57–70, 2000.

[8] Gerald W. Prager, Marina Poettler, Matthias Unseld, and Christoph C. Zielinski. Angiogenesis in cancer: anti-vegf escape mechanisms. *Translational lung cancer research*, 1:14–25, 2012.

[9] Gerald McMahon. Vegf receptor signaling in tumor angiogenesis. *The Oncologist*, 5:3–10, 2000.

[10] Yasuhiro Matsumura and Hiroshi Maeda. A new concept for macromolecular therapeutics in cancer chemotherapy: Mechanism of tumoritropic accumulation of proteins and the antitumor agent smancs. *Cancer Reasearch*, 46: 6387–6392, 1986.

[11] Uma Prabhakar, Hiroshi Maeda, and Rakesh K. Jain. Challenges and key considerations of the enhanced permeability and retention effect for nanomedicine drug delivery in oncology. *Cancer Reasearch*, 73:2412–2417, 2013.

[12] Khaled Greish. Enhanced permeability and retention of macromolecular drugs in solid tumors: A royal gate for targeted anticancer nanomedicines. *Journal of drug targeting*, 15:457–464, 2007.

[13] Pengfei Lu, Valerie M. Weaver, and Zena Werb. The extracellular matrix: A dynamic niche in cancer progression. *Journal of cell biology*, 196:395–406, 2012.

[14] Matthew J. Paszek, Nastaran Zahir, Kandice R. Johnson, Johnathon N. Lakins, Gabriela I. Rozenberg, Amit Gefen, Cynthia A. Reinhart-King, Susan S. Margulies, Micah Dembo, David Boettiger, Daniel A. Hammer, and Valerie M. Weaver. Tensional homeostasis and the malignant phenotype. *Cancer Cell*, 8:241–254, 2000.

[15] Matthew J. Paszek, Nastaran Zahir, Kandice R. Johnson, Johnathon N. Lakins, Gabriela I. Rozenberg, Amit Gefen, Cynthia A. Reinhart-King, Susan S. Margulies, Micah Dembo, David Boettiger, Daniel A. Hammer, and Valerie M. Weaver. Tensional homeostasis and the malignant phenotype. *Cancer cell*, 8:241–254, 2005.

[16] Paolo A. Netti, David A. Berk, Melody A. Swartz, Alan J. Grodzinsky, and Rakesh K. Jain. Role of extracellular matrix assembly in interstitial transport in solid tumors. *Cancer Research*, 60:2497–2503, 2000.

[17] Leslie O. Simpson. Basement membranes and biological thixotropy: A new hypothesis. *Pathology*, 12:377–389, 1980.

[18] Bjørn A. J. Angelsen. *Ultrasound imaging - Waves, signals, and signal processing*. Emantec AS, 2000.

[19] Trond Varslot and Gunnar Taraldsen. Computer simulation of forward wave propagation in soft tissue. *IEEE Transactions on ultrasonics, ferroelectrics, and frequency control*, 50:1473–1482, 2005.

[20] Fabrice Prieur, Tonni Franke Johansen, Sverre Holm, and Hans Torp. Fast simulation of second harmonic ultrasound field using a quasi-linear method. *The Journal of the Acoustic Society of America*, 131:4365–4375, 2012.

[21] Johannes Kvam. Fast simulation of surf ultrasound transmit pulse complexes using heterogeneous computing platforms. Master's thesis, NTNU, 2012.

[22] Joshua R. Doherty, gregg E. Trahey, Kathryn R. Nightingale, and Mark. L. Palmeri. Acoustic radiation force elasticity imaging in diagnostic ultrasound. *IEEE Transactions on Ultrasonics, Ferroelectronics and Frequency Control*, 60:685–701, 2013.

[23] Mark. L. Palmeri, Amy C. Sharma, and Kathryn R. Nightingale. A finite-element method model of soft tissue response to impulsive acoustic radiation force. *IEEE Transactions on Ultrasonics, Ferroelectronics and Frequency Control*, 52:1699–1712, 2005.

[24] J. N. Reddy. *An Introduction to Continuum Mechanics with applications*. Cambridge University Press, 2 edition, 2008.

[25] James A. Fay. *Introduction to Fluid Mechanics*. The MIT Press, 2 edition, 1998.

[26] Mark F. Hamilton and David T. Blackstock. *Nonlinear acoustics*. Acoustical Society of America, 2 edition, 2008.

[27] Bjørn Angelsen. Ultrasound radiation force transport of drugs in tumors. *Department of Circulation and Medical Imaging, NTNU*, 2013.

[28] Richard S. C. Cobbold. *Foundations of Biomedical Ultrasound*. Oxford University Press, 2007.

[29] Osama. M. Hassan, Noha. S. D. Hassan, and Yasser. M. Kadah. Modeling of ultrasound hyperthermia treatment of breast tumors. *26th National radio science conference*, pages 1–8, 2009.

[30] Paul M. Meaney, Robert L. Clarke, Gail R. ter Haar, and Ian H. Rivens. A 3-d finite-element model for computation of temperature profiles and regions of thermal damage during focused ultrasound surgery exposures. *Ultrasound in Medicine and Biology*, 24:1489–1489, 1998.

[31] Morton W. Miller and Marvin C. Ziskin. Biological consequences of hyperthermia. *Ultrasound in Medicine and Biology*, 8:707–722, 1989.

[32] Stanley B Barnett, Gail R Ter Haar, Marvin C. Ziskin, Hans-Dieter Rott, Francis A Duck, and Kazuo Maeda. International recommendations and guidelines for the safe use of diagnostic ultrasound in medicine. *Ultrasound in Medicine and Biology*, 26:355–366, 2000.

[33] Olympus NDT Inc. Harasonic transducers.

[34] Wen-Chen Lin, Chih-Chieh Wu, Tzung-Chi Huang, Wen-Chi lin, Bill Yuan-Chi Chiu, Ren-Shyan Liu, and Kang-Ping Lin. Red blood cell velocity measurement in rodent tumor model: An in vivo microscopic study. *Journal of Medical and Biological Engineering*, 32:97–102, 2012.

[35] Paul Dayton, Alexander Klibanov, Gary Brandenburger, and Kathy Ferrara. Acoustic radiation force in vivo: a mechanism to assist targeting of microbubbles. *Ultrasound in Medicine and Biology*, 25:1195–1201, 1999.

[36] Yao-Sheng Tung, Fotios Vlachos, James J. Choi, Thomas Deffieux, Kirsten Selert, and Elisa E. Konofagou. In vivo transcranial cavitation threshold detection during ultrasound-induced blood-brain barrier opening in mice. *Ultrasound in Medicine and Biology*, 55:6141–6155, 2010.

[37] Victor F. Humphrey. Nonlinear propagation in ultrasonic fields: measurements, modelling and harmonic imaging. *Ultrasonics*, 38:267–272, 2000.

[38] Francis A. Duck. Nonlinear acoustics in diagnostic ultrasound. *Ultrasound in Medicine and Biology*, 28:1–18, 2002.